

Traumatic Brain-and-Spine Injury Mechanics Supported by the Crash Simulator Toolbox

Vladimir G. Ivancevic^{1,*} and Shady Mohamed²

¹Joint and Operations Analysis Division, Defence Science & Technology Organisation, Australia

²Centre for Intelligent Systems Research, Deakin University, Australia

Abstract: Recently, the first author has proposed a new coupled-loading-rate hypothesis as a unique cause of both brain and spinal injuries, which states that they are both caused by a Euclidean jolt, an impulsive loading that strikes head and spine (or, any other part of the human body)- in several coupled degrees-of-freedom simultaneously. Injury never happens in a single direction only, nor is it ever caused by a static force. It is always an impulsive translational plus rotational force. The Euclidean jolt causes two basic forms of brain, spine and other musculo-skeletal injuries: (i) localized translational dislocations; and (ii) localized rotational disclinations. In the present paper, we first review this unique mechanics of a general human mechanical neuro-musculo-skeletal injury, and then describe how it can be predicted and controlled by the new crash simulator toolbox. This rigorous *Matlab* toolbox has been developed using an existing third-party toolbox *DiffMan*, for accurately solving differential equations on smooth manifolds and mechanical Lie groups. The present crash simulator toolbox performs prediction and control of brain and spinal injuries within the framework of the Euclidean group SE(3) of general rigid body motions.

Keywords: Traumatic brain injury, spinal injury, biomechanics, simulation, Matlab toolbox.

1. INTRODUCTION

Prediction and prevention of traumatic brain injury and spinal injury, as well as general musculo-skeletal injury, is a very important aspect of preventive medical science. In a series of papers [1-4], the first author of the present article proposed a new coupled loading-rate hypothesis as a unique cause of all above injuries. This new hypothesis states that the main cause of all mechanical injuries is a Euclidean Jolt, which is an impulsive loading that strikes any part of the human body (head, spine or any bone/joint)- in several coupled degrees-of-freedom simultaneously. It never goes in a single direction only. Also, it is never a static force. It is always an impulsive translational and rotational force coupled to some mass eccentricity.

To show this, based on the previously defined *covariant force law* [5-7], we have firstly formulated the fully coupled Newton-Euler dynamics of:

1. Brain's micro-motions within the cerebrospinal fluid inside the cranial cavity;
2. Any local inter-vertebral motions along the spine; and
3. Any major joint motions in the human musculo-skeletal system.

Then, from it, we have defined the essential concept of *Euclidean Jolt*, which is the main cause of all mechanical human injuries. The Euclidean Jolt has two main components:

- Sudden motion, caused either by an accidental impact or slightly distorted human movement; and
- Unnatural mass distribution of the human body (possibly with some added external masses), which causes some mass eccentricity from the natural physiological body state.

This can be intuitively (in plain English) explained in the following way. As we live in a (Euclidean) 3D space, one could think that motion of any part of the human body, caused either by a voluntary human movement, or by an accidental impact, simply obeys classical mechanics in 6 degrees-of-freedom: three translations and three rotations. However, these 6 degrees-of-freedom are not independent motions as it is suggested by the standard term degrees-of-freedom. In reality, these six motions of any body in space are coupled. Firstly, three rotations are coupled in the so-called rotation group (or matrix, or quaternion). Secondly, three translations are coupled with the rotation group to give the full Euclidean group of rigid body motions in space. A simple way to see this is to observe someone throwing an object in the air or hitting a tennis ball: how far and where it will fly depends not only on the standard projectile mechanics, but also on its local spin around all three axes simultaneously.

*Address correspondence to this author at the Joint and Operations Analysis Division, Defence Science & Technology Organisation, Australia;
Tel: +61-8-7389-7337; Fax: +61-8-7389-4193;
E-mail: Vladimir.Ivancevic@dsto.defence.gov.au

Every golf and tennis player knows this simple fact. Once the spin is properly defined we have a fully coupled Newton-Euler dynamics- to start with.

The covariant force law for any biodynamical system goes one step beyond the Newton-Euler dynamics. It states:

Euclidean Force covector field

= **Body mass distribution** \times

Euclidean Acceleration vector field

This is a nontrivial biomechanical generalization of the fundamental Newton's definition of the force acting on a single particle. Unlike classical engineering mechanics of multi-body systems, this fundamental law of biomechanics proposes that forces acting on a multi-body system and causing its motions are fundamentally different physical quantities from the resulting accelerations. In simple words, forces are massive quantities while accelerations are massless quantities. More precisely, the acceleration vector field includes all linear and angular accelerations of individual body segments. When we couple them all with the total body's mass-distribution matrix of all body segments (including all masses and inertia moments), we get the force co-vector field, comprising all the forces and torques acting on the individual body segments. In this way, we have defined the 6-dimensional Euclidean force for an arbitrary biomechanical system.

Now, for prediction of injuries, we need to take the rate-of-change (or derivative, with respect to time) of the Euclidean biomechanical force defined above. In this way, we get the Euclidean Jolt, which is the sudden change (in time) of the 6-dimensional Euclidean force:

Euclidean Jolt covector field

= **Body mass distribution** \times **Euclidean Jerk vector field**

And again, it consists of two components: (i) massless linear and angular jerks (of all included body segments), and (ii) their mass distribution. For the sake of simplicity, we can say that the mass distribution matrix includes all involved segmental masses and inertia moments, as well as eccentricities or pathological leverages from the normal physiological state.

Therefore, the unique cause of all brain, spine and musculo-skeletal injuries has two components:

- Coupled linear and angular jerks; and

- Mass distribution with eccentricities.

In other words, *there are no injuries in static conditions without any mass eccentricities; all injuries are caused by mutually coupled linear and angular jerks, which are also coupled with the involved mass distribution.*

The Euclidean Jolt causes two forms of discontinuous brain, spine or musculo-skeletal injury:

1. Mild rotational disclinations; and
2. Severe translational dislocations and/or bone fractures.

In the cited papers above, we have developed the soft-body dynamics of biomechanical disclinations and dislocations, caused by the Euclidean Jolt, using the Cosserat multipolar viscoelastic continuum model.

Implications of the new universal theory are various, as follows.

A. The research in traumatic brain injury (TBI, see Figure 1) has so far identified the rotation of the brain-stem as the main cause of the TBI due to various crashes/impacts. The contribution of my universal Jolt theory to the TBI research is the following:

1. Rigorously defined this brain rotation as a mechanical disclination of the brain-stem tissue modelled by the Cosserat multipolar soft-body model;
2. Showing that brain rotation is never uni-axial but always three-axial;
3. Showing that brain rotation is always coupled with translational dislocations. This is a straightforward consequence of my universal Jolt theory.

These apparently 'obvious' facts are actually *radically new*: we cannot separately analyze rapid brain's rotations from translations, because they are in reality always coupled.

One practical application of the brain Jolt theory is in design of helmets. Briefly, a 'hard' helmet saves the skull but not the brain; alternatively, a 'soft' helmet protects the brain from the collision jolt but does not protect the skull. A good helmet is both 'hard' and 'soft'. A proper helmet would need to have both a hard external shell (to protect the skull) and a soft internal part (that will dissipate the energy from the collision jolt by its own destruction, in the same way as a car saves

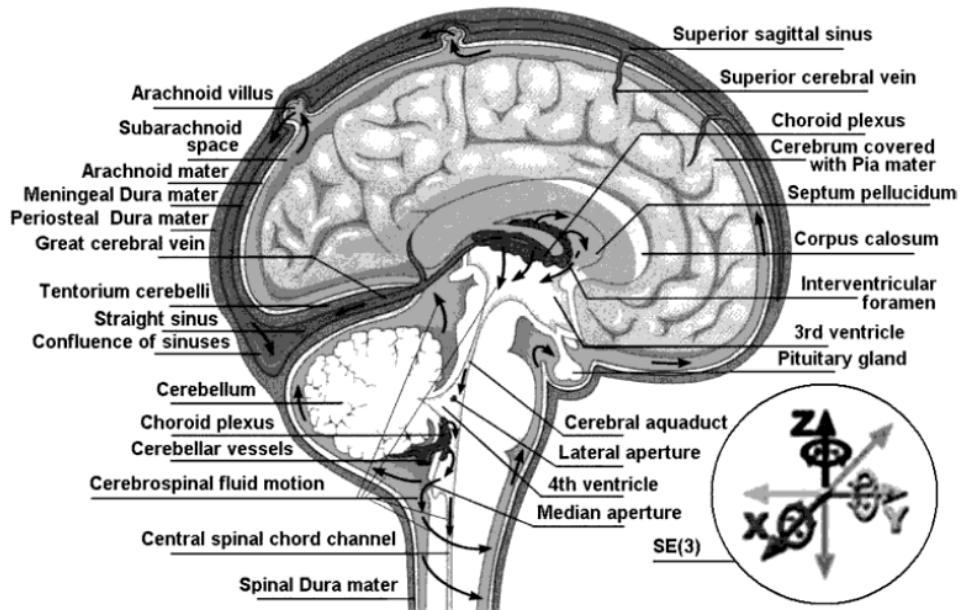


Figure 1: Human brain and its SE(3)-group of microscopic three-dimensional motions within the cerebrospinal fluid inside the cranial cavity.

its passengers from the collision jolt by its own destruction).

Similarly, in designing safer car air-bags, the two critical points will be (i) their placement within the car, and (ii) their soft-hard characteristics, similar to the helmet characteristics described above.

B. In case of spinal injury (see Figure 2), the contribution of my universal Jolt theory is the following:

1. The spinal injury is always localized at the certain vertebral or inter-vertebral point;

2. In case of severe translational injuries (vertebral fractures or discus herniae) they can be identified using X-ray or other medical imaging scans; in case of microscopic rotational injuries (causing the back-pain syndrome) they cannot be identified using current medical imaging scans;
3. There is no spinal injury without one of the following two causes:
 - a. Impulsive rotational + translational loading caused by either fast human movements or various crashes/impacts; and/or

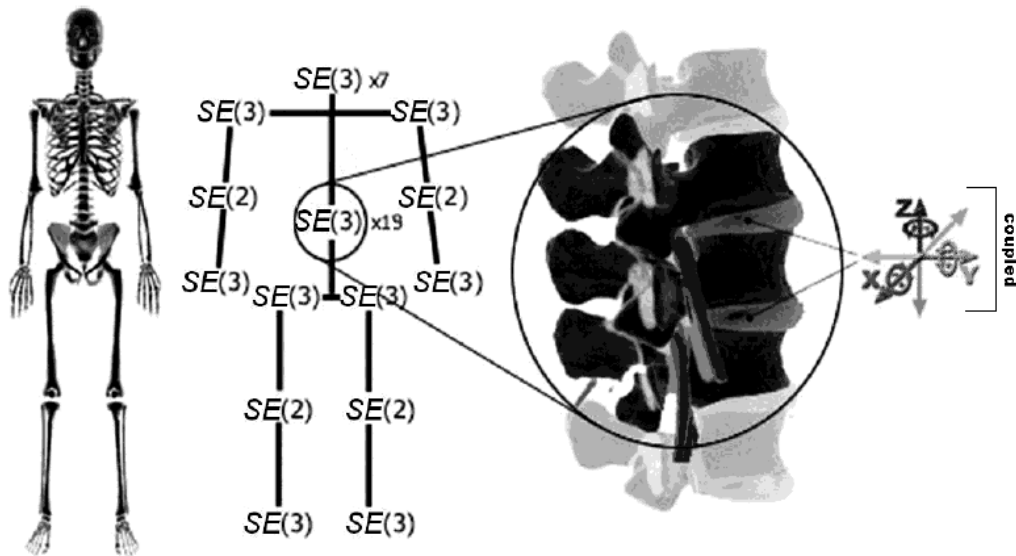


Figure 2: Human body representation in terms of SE(3)/SE(2)-groups of rigid-body motion, with the vertebral column represented as a chain of 26 flexibly-coupled SE(3)-groups.

- b. Static eccentricity from the normal physiological spinal form, caused by external loading;
- c. Any spinal injury is caused by a combination of the two points above: impulsive rotational + translational loading and static eccentricity.

This is a straightforward consequence of my universal Jolt theory. We cannot separately analyze translational and rotational spinal injuries. Also, there are no static injuries without eccentricity. Indian women have for centuries carried bulky loads on their heads without any spinal injuries; they just prevented any load eccentricities and any jerks in their motion.

The currently used Principal loading hypothesis that describes spinal injuries in terms of spinal tension, compression, bending, and shear, covers only a small subset of all spinal injuries covered by my universal Jolt theory. To prevent spinal injuries we need to develop spinal jolt awareness: ability to control all possible impulsive spinal loadings as well as static eccentricities.

C. In case of general musculo-skeletal injury, the contribution of my universal Jolt theory is the following:

1. The injury is always localized at the certain joint or bone and caused by an impulsive loading, which hits this particular joint/bone in several coupled degrees-of-freedom simultaneously;
2. Injury happens when most of the body mass is hanging on that joint; for example, in case of a knee injury, when most of the body mass is on one leg with a semi-flexed knee- and then, caused by some external shock, the knee suddenly jerks (this can happen in running, skiing, and ball games, as well as various crashes/impacts); or, in case of shoulder injury, when most of the body mass is hanging on one arm and then it suddenly jerks.

To prevent all these injuries we need to develop musculo-skeletal jolt awareness. For example, never overload a flexed knee and avoid any kind of uncontrolled motions (like slipping) or collisions with external objects.

In this paper, we propose two things: firstly, a universal theory of brain-and-spine injury prediction and prevention; and secondly, a *Matlab*TM crash-simulator toolbox for prediction of brain-and-spine injury.

2. BRAIN-AND-SPINE INJURY

2.1. Traumatic Brain Injury Mechanics

Traumatic brain injury (TBI) is still a major health problem, with over a half-a-million cases per year, mostly caused by motor-vehicle accidents (frequently involving alcohol use). TBI occurs when physical trauma causes brain damage, which can result from a closed head injury¹ or a penetrating head injury.² In both cases, TBI is caused by rapid deformation of the brain, resulting in a cascade of pathological events and ultimately neuro-degeneration.³ Parts of the brain that can be damaged include the cerebral hemispheres, cerebellum, and brain stem. TBI can cause a host of physical, cognitive, emotional, and social effects. TBI is a frequent cause of major long-term disability in individuals surviving head injuries sustained in war zones. This is becoming an issue of growing concern in modern warfare in which rapid deployment of acute interventions are effective in saving the lives of combatants with significant head injuries. Traumatic brain injury has been identified as the 'signature injury' among wounded soldiers of military engagement. Rapid deformation of brain matter caused by skull acceleration is most likely the cause of concussion, as well as more severe TBI. The inability to measure deformation directly has led to disagreement and confusion about the biomechanics of concussion and TBI (see [1] and references therein).

TBI can be mild, moderate, or severe (depending on the extent of the damage to the brain), while the final outcome can be anything from complete recovery to permanent disability or death (see [8]). Some symptoms are evident immediately, while others do not surface until several days or weeks after the injury⁴ (see [9]).

¹A closed injury occurs when the head suddenly and violently hits an object but the object does not break through the skull.

²A penetrating injury occurs when an object pierces the skull and enters brain tissue.

³In many cases of TBI widespread disruption of the axons occurs through a process known as diffuse axonal injury (DAI) or traumatic axonal injury (TAI).

⁴With mild TBI, the patient may remain conscious or may lose consciousness for a few seconds or minutes; the person may also feel dazed or not like him- or herself for several days or weeks after the initial injury; other symptoms include: headache, mental confusion, lightheadedness, dizziness, double vision, blurred vision (or tired eyes), ringing in the ears, bad taste in the mouth, fatigue or lethargy, a change in sleep patterns, behavioral or mood changes, trouble with memory/concentration/calculation. With moderate or severe TBI, the patient may show these same symptoms, but may also have: loss of consciousness, personality change, a severe/persistent/worsening headache, repeated vomiting/nausea, seizures, inability to awaken, dilation (widening) of one or both pupils, slurred speech, weakness/numbness in the extremities, loss of coordination, increased confusion, restlessness/agitation; vomiting and neurological deficit together are important indicators of prognosis and their presence may warrant early CT scanning and neurosurgical intervention.

The natural cushion that protects the brain from trauma is the *cerebrospinal fluid* (CSF). It resides within cranial and spinal cavities and moves in a pulsatile fashion to and from the cranial cavity (see Figure 1). This motion can be measured by functional magnetic resonance imaging (fMRI, see [10] for a review) and may be of clinical importance in the diagnosis of several brain and spinal cord disorders such as hydrocephalus, Chiari malformation, and syringomyelia. It was found in [11] that brain and CSF of healthy volunteers exhibited periodic motion in the frequency range of normal heart rate. Both brain hemispheres showed periodic squeezing of the ventricles, with peak velocities up to 1 mm/sec followed by a slower recoil. Superimposed on the regular displacement of the brain stem was a slow, respiratory-related periodic shift of the neutral position. During the Valsalva maneuver, the brain stem showed initial caudal and subsequent cranial displacement of 2-3 mm. Coughing produced a short swing of CSF in the cephalic direction. The pressure gradient waveform of a linearized Navier-Stokes model of the pulsatile CSF flow was found in [12] to be almost exclusively dependent on the flow waveform and cross-sectional area.

The microscopic motion of human brain within the skull is, in the language of modern dynamics [5-7], governed by the Euclidean SE(3)-group of 3D motions. Within brain's SE(3)-group we have both SE(3)-kinematics (consisting of SE(3)-velocity and its two time derivatives: SE(3)-acceleration and SE(3)-jerk) and SE(3)-dynamics (consisting of SE(3)-momentum and its two time derivatives: SE(3)-force and SE(3)-jolt), which is brain's kinematics \times brain's mass-inertia distribution.

As already explained, the external SE(3)-jolt⁵ is a sharp and sudden change in the SE(3)-force acting on brain's mass-inertia distribution (given by brain's mass and inertia matrices). That is, a 'delta'-change in a 3D force-vector coupled to a 3D torque-vector, striking the head-shell with the brain immersed into the cerebrospinal fluid. In other words, the SE(3)-jolt is a sudden, sharp and discontinues shock in all 6 coupled

dimensions of brain's continuous micro-motion within the cerebrospinal fluid (see Figure 1), namely within the three Cartesian (x, y, z) -translations and the three corresponding Euler angles around the Cartesian axes: roll, pitch and yaw. If the SE(3)-jolt produces a mild shock to the brain (e.g., strong head shake), it causes mild TBI, with temporary disabled associated sensory-motor and/or cognitive functions and affecting respiration and movement. If the SE(3)-jolt produces a hard shock (hitting the head with external mass), it causes severe TBI, with the total loss of gesture, speech and movement.

The SE(3)-jolt is rigorously defined in terms of differential geometry [7, 13]. Briefly, it is the absolute time-derivative of the covariant force 1-form (or, co-vector field). As already stated, the fundamental law of biomechanics is the covariant force law:

$$\text{Force co-vector field} = \text{Mass distribution} \times \text{Acceleration vector-field},$$

which is formally written (using the Einstein summation convention, with indices labelling the three Cartesian translations and the three corresponding Euler angles):

$$F_{\mu} = m_{\mu\nu} a^{\nu}, \quad (\mu, \nu = 1, \dots, 6)$$

where F_{μ} denotes the 6 covariant components of the external pushing SE(3)-force co-vector field, $m_{\mu\nu}$ represents the 6×6 covariant components of brain's inertia-metric tensor, while a^{ν} corresponds to the 6 contravariant components of brain's internal SE(3)-acceleration vector-field.

Now, the covariant (absolute, Bianchi) time-derivative $\frac{D}{dt}(\cdot)$ of the covariant SE(3)-force F_{μ} defines the corresponding external "striking" SE(3)-jolt co-vector field:

$$\frac{D}{dt}(F_{\mu}) = m_{\mu\nu} \frac{D}{dt}(a^{\nu}) = m_{\mu\nu} \left(\dot{a}^{\nu} + \Gamma_{\mu\lambda}^{\nu} a^{\lambda} \right), \quad (1)$$

where $\frac{D}{dt}(a^{\nu})$ denotes the 6 contravariant components of brain's internal SE(3)-jerk vector-field and overdot $(\dot{\cdot})$ denotes the time derivative. $\Gamma_{\mu\lambda}^{\nu}$ are the Christoffel's symbols of the Levi-Civita connection for the SE(3)-group, which are zero in case of pure Cartesian translations and nonzero in case of rotations as well as in the full-coupling of translations and rotations.

In the following, we elaborate on the SE(3)-jolt concept (using vector and tensor methods) and its

⁵The mechanical SE(3)-jolt concept is based on the mathematical concept of higher-order tangency (rigorously defined in terms of jet bundles of the head's configuration manifold) [7, 13], as follows: When something hits the human head, or the head hits some external body, we have a collision. This is naturally described by the SE(3)-momentum, which is a nonlinear coupling of 3 linear Newtonian momenta with 3 angular Eulerian momenta. The tangent to the SE(3)-momentum, defined by the (absolute) time derivative, is the SE(3)-force. The second-order tangency is given by the SE(3)-jolt, which is the tangent to the SE(3)-force, also defined by the time derivative.

biophysical TBI consequences in the form of brain's dislocations and disclinations.

2.1.1. *SE(3)-Group of Brain's Micro-Motions within the CSF*

The brain and the CSF together exhibit periodic microscopic translational and rotational motion in a pulsatile fashion to and from the cranial cavity, in the frequency range of normal heart rate (with associated periodic squeezing of brain's ventricles) [11]. This micro-motion is mathematically defined by the Euclidean (gauge) $SE(3)$ -group. Briefly, the $SE(3)$ -group is defined as a semidirect (noncommutative) product \triangleright of 3D rotations and 3D translations:

$$SE(3) := SO(3) \triangleright \mathbb{R}^3.$$

Its most important subgroups are the following (see Appendix for technical details):

Subgroup	Definition
$SO(3)$, group of rotations in 3D (a spherical joint)	Set of all proper orthogonal 3×3 - rotational matrices
$SE(2)$, special Euclidean group in 2D (all planar motions)	Set of all 3×3 - matrices: $\begin{bmatrix} \cos\theta & \sin\theta & r_x \\ -\sin\theta & \cos\theta & r_y \\ 0 & 0 & 1 \end{bmatrix}$
$SO(2)$, group of rotations in 2D subgroup of $SE(2)$ -group (a revolute joint)	Set of all proper orthogonal 2×2 - rotational matrices included in $SE(2)$ - group
\mathbb{R}^3 , group of translations in 3D (all spatial displacements)	Euclidean 3D vector space

In other words, the gauge $SE(3)$ -group of Euclidean micro-motions of the brain immersed in the cerebrospinal fluid within the cranial cavity, contains matrices of the form $\begin{pmatrix} \mathbf{R} & \mathbf{b} \\ 0 & 1 \end{pmatrix}$, where \mathbf{b} is brain's 3D micro-translation vector and \mathbf{R} is brain's 3D rotation matrix, given by the product $\mathbf{R} = R_\varphi \cdot R_\psi \cdot R_\theta$ of brain's three Eulerian micro-rotations, roll = R_φ , pitch = R_ψ , yaw = R_θ , performed respectively about the x -axis by an angle φ , about the y -axis by an angle ψ , and about the z -axis by an angle θ [5-7, 14, 15]:

$$R_\varphi = \begin{bmatrix} 1 & 0 & 0 \\ 0 & \cos\varphi & -\sin\varphi \\ 0 & \sin\varphi & \cos\varphi \end{bmatrix}, \quad R_\psi = \begin{bmatrix} \cos\psi & 0 & \sin\psi \\ 0 & 1 & 0 \\ -\sin\psi & 0 & \cos\psi \end{bmatrix},$$

$$R_\theta = \begin{bmatrix} \cos\theta & -\sin\theta & 0 \\ \sin\theta & \cos\theta & 0 \\ 0 & 0 & 1 \end{bmatrix}.$$

Therefore, brain's natural $SE(3)$ -dynamics within the cerebrospinal fluid is given by the coupling of Newtonian (translational) and Eulerian (rotational) equations of micro-motion.

2.1.2. *Brain's Natural SE(3)-Dynamics*

To support our coupled loading-rate hypothesis, we formulate the coupled Newton-Euler dynamics of brain's micro-motions within the skull's $SE(3)$ -group of motions. The forced Newton-Euler equations read in vector (boldface) form

$$\begin{aligned} \text{Newton: } \dot{\mathbf{p}} &\equiv \mathbf{M}\dot{\mathbf{v}} = \mathbf{F} + \mathbf{p} \times \boldsymbol{\omega}, \\ \text{Euler: } \dot{\boldsymbol{\pi}} &\equiv \mathbf{I}\dot{\boldsymbol{\omega}} = \mathbf{T} + \boldsymbol{\pi} \times \boldsymbol{\omega} + \mathbf{p} \times \mathbf{v}, \end{aligned} \quad (2)$$

where \times denotes the vector cross product,⁶

$$\begin{aligned} \mathbf{M} &\equiv M_{ij} = \text{diag}\{m_1, m_2, m_3\} \quad \text{and} \\ \mathbf{I} &\equiv I_{ij} = \text{diag}\{I_1, I_2, I_3\}, \quad (i, j = 1, 2, 3) \end{aligned}$$

are brain's (diagonal) mass and inertia matrices,⁷ defining brain's mass-inertia distribution, with principal inertia moments given in Cartesian coordinates (x, y, z) by volume integrals

$$\begin{aligned} I_1 &= \iiint \rho(z^2 + y^2) dx dy dz, \quad I_2 = \iiint \rho(x^2 + z^2) dx dy dz, \\ I_3 &= \iiint \rho(x^2 + y^2) dx dy dz, \end{aligned}$$

dependent on brain's density $\rho = \rho(x, y, z)$,

$$\mathbf{v} \equiv \mathbf{v}^i = [v_1, v_2, v_3]^t \quad \text{and} \quad \boldsymbol{\omega} \equiv \boldsymbol{\omega}^i = [\omega_1, \omega_2, \omega_3]^t$$

⁶Recall that the cross product $\mathbf{u} \times \mathbf{v}$ of two vectors \mathbf{u} and \mathbf{v} equals $\mathbf{u} \times \mathbf{v} = uv \sin\theta \mathbf{n}$, where θ is the angle between \mathbf{u} and \mathbf{v} , while \mathbf{n} is a unit vector perpendicular to the plane of \mathbf{u} and \mathbf{v} such that \mathbf{u} and \mathbf{v} form a right-handed system.

⁷In reality, mass and inertia matrices (\mathbf{M}, \mathbf{I}) are not diagonal but rather full 3×3 positive-definite symmetric matrices with coupled mass- and inertia-products. Even more realistic, fully-coupled mass-inertia properties of a brain immersed in (incompressible, irrotational and inviscid) cerebrospinal fluid are defined by the single non-diagonal 6×6 positive-definite symmetric mass-inertia matrix $\mathbf{M}_{SE(3)}$, the so-called material metric tensor of the $SE(3)$ -group, which has all nonzero mass-inertia coupling products. In other words, the 6×6 matrix $\mathbf{M}_{SE(3)}$ contains: (i) brain's own mass plus the added mass matrix associated with the fluid, (ii) brain's own inertia plus the added inertia matrix associated with the potential flow of the fluid, and (iii) all the coupling terms between linear and angular momenta. However, for simplicity, in this paper we shall consider only the simple case of two separate diagonal 3×3 matrices (\mathbf{M}, \mathbf{I}) .

(where $[\]^t$ denotes the vector transpose) are brain's linear and angular velocity vectors (that is, column vectors),

$$\mathbf{F} \equiv F_i = [F_1, F_2, F_3] \quad \text{and} \quad \mathbf{T} \equiv T_i = [T_1, T_2, T_3]$$

are gravitational and other external force and torque co-vectors (that is, row vectors) acting on the brain within the skull,

$$\mathbf{p} \equiv p_i \equiv \mathbf{M}\mathbf{v} = [p_1, p_2, p_3] = [m_1 v_1, m_2 v_2, m_3 v_3] \quad \text{and}$$

$$\boldsymbol{\pi} \equiv \pi_i \equiv \mathbf{I}\boldsymbol{\omega} = [\pi_1, \pi_2, \pi_3] = [I_1 \omega_1, I_2 \omega_2, I_3 \omega_3]$$

are brain's linear and angular momentum co-vectors.

In tensor form, the forced Newton-Euler equations (2) read:

$$\dot{p}_i \equiv M_{ij} \dot{v}^j = F_i + \varepsilon_{ik}^j p_j \omega^k, \quad (i, j, k = 1, 2, 3)$$

$$\dot{\pi}_i \equiv I_{ij} \dot{\omega}^j = T_i + \varepsilon_{ik}^j \pi_j \omega^k + \varepsilon_{ik}^j p_j v^k,$$

where the permutation symbol ε_{ik}^j is defined as:

$$\varepsilon_{ik}^j = \begin{cases} +1 & \text{if } (i, j, k) \text{ is } (1, 2, 3), (3, 1, 2) \text{ or } (2, 3, 1), \\ -1 & \text{if } (i, j, k) \text{ is } (3, 2, 1), (1, 3, 2) \text{ or } (2, 1, 3), \\ 0 & \text{otherwise: } i = j \text{ or } j = k \text{ or } k = i. \end{cases}$$

In scalar form, the forced Newton-Euler equations (2) expand as

$$\text{Newton: } \begin{cases} \dot{p}_1 = F_1 - m_3 v_3 \omega_2 + m_2 v_2 \omega_3 \\ \dot{p}_2 = F_2 + m_3 v_3 \omega_1 - m_1 v_1 \omega_3 \\ \dot{p}_3 = F_3 - m_2 v_2 \omega_1 + m_1 v_1 \omega_2 \end{cases} \quad (3)$$

$$\text{Euler: } \begin{cases} \dot{\pi}_1 = T_1 + (m_2 - m_3) v_2 v_3 + (I_2 - I_3) \omega_2 \omega_3 \\ \dot{\pi}_2 = T_2 + (m_3 - m_1) v_1 v_3 + (I_3 - I_1) \omega_1 \omega_3 \\ \dot{\pi}_3 = T_3 + (m_1 - m_2) v_1 v_2 + (I_1 - I_2) \omega_1 \omega_2 \end{cases}$$

showing brain's individual mass and inertia couplings.

Equations (2)-(3) can be derived from the translational + rotational kinetic energy of the brain⁸

$$E_k = \frac{1}{2} \mathbf{v}^t \mathbf{M} \mathbf{v} + \frac{1}{2} \boldsymbol{\omega}^t \mathbf{I} \boldsymbol{\omega}, \quad (4)$$

⁸In a fully-coupled Newton-Euler brain dynamics, instead of equation (Ek) we would have brain's kinetic energy defined by the inner product:

$$E_k = \frac{1}{2} \begin{pmatrix} \mathbf{p} \\ \boldsymbol{\pi} \end{pmatrix} \mathbf{M}_{SE(3)} \begin{pmatrix} \mathbf{p} \\ \boldsymbol{\pi} \end{pmatrix}.$$

or, in tensor form

$$E = \frac{1}{2} M_{ij} v^i v^j + \frac{1}{2} I_{ij} \omega^i \omega^j.$$

For this we use the *Kirchhoff-Lagrangian equations* (see [1] and references therein):

$$\frac{d}{dt} \partial_{\mathbf{v}} E_k = \partial_{\mathbf{v}} E_k \times \boldsymbol{\omega} + \mathbf{F},$$

$$\frac{d}{dt} \partial_{\boldsymbol{\omega}} E_k = \partial_{\boldsymbol{\omega}} E_k \times \boldsymbol{\omega} + \partial_{\mathbf{v}} E_k \times \mathbf{v} + \mathbf{T}, \quad (5)$$

where $\partial_{\mathbf{v}} E_k = \frac{\partial E_k}{\partial \mathbf{v}}$, $\partial_{\boldsymbol{\omega}} E_k = \frac{\partial E_k}{\partial \boldsymbol{\omega}}$; in tensor form these equations read

$$\frac{d}{dt} \partial_{v^i} E = \varepsilon_{ik}^j (\partial_{v^j} E) \omega^k + F_i,$$

$$\frac{d}{dt} \partial_{\omega^i} E = \varepsilon_{ik}^j (\partial_{\omega^j} E) \omega^k + \varepsilon_{ik}^j (\partial_{v^j} E) v^k + T_i.$$

Using (4)-(5), brain's linear and angular momentum co-vectors are defined as

$$\mathbf{p} = \partial_{\mathbf{v}} E_k, \quad \boldsymbol{\pi} = \partial_{\boldsymbol{\omega}} E_k,$$

or, in tensor form

$$p_i = \partial_{v^i} E, \quad \pi_i = \partial_{\omega^i} E,$$

with their corresponding time derivatives, in vector form

$$\dot{\mathbf{p}} = \frac{d}{dt} \mathbf{p} = \frac{d}{dt} \partial_{\mathbf{v}} E, \quad \dot{\boldsymbol{\pi}} = \frac{d}{dt} \boldsymbol{\pi} = \frac{d}{dt} \partial_{\boldsymbol{\omega}} E,$$

or, in tensor form

$$\dot{p}_i = \frac{d}{dt} p_i = \frac{d}{dt} \partial_{v^i} E, \quad \dot{\pi}_i = \frac{d}{dt} \pi_i = \frac{d}{dt} \partial_{\omega^i} E,$$

or, in scalar form

$$\dot{\mathbf{p}} = [\dot{p}_1, \dot{p}_2, \dot{p}_3] = [m_1 \dot{v}_1, m_2 \dot{v}_2, m_3 \dot{v}_3],$$

$$\dot{\boldsymbol{\pi}} = [\dot{\pi}_1, \dot{\pi}_2, \dot{\pi}_3] = [I_1 \dot{\omega}_1, I_2 \dot{\omega}_2, I_3 \dot{\omega}_3].$$

While brain's healthy *SE(3)*-dynamics within the cerebrospinal fluid is given by the coupled Newton-Euler micro-dynamics, the TBI is actually caused by the sharp and discontinuous change in this natural *SE(3)* micro-dynamics, in the form of the *SE(3)*-jolt, causing brain's discontinuous deformations.

2.1.3. Brain's Traumatic Dynamics: the *SE(3)*-jolt

The *SE(3)*-jolt, the actual cause of the TBI (in the form of the brain's plastic deformations), is defined as a

coupled Newton+Euler jolt; in (co)vector form the $SE(3)$ -jolt reads⁹

$$SE(3)\text{-jolt} : \begin{cases} \text{Newton jolt} : \dot{\mathbf{F}} = \ddot{\mathbf{p}} - \dot{\mathbf{p}} \times \boldsymbol{\omega} - \mathbf{p} \times \dot{\boldsymbol{\omega}}, \\ \text{Euler jolt} : \dot{\mathbf{T}} = \ddot{\boldsymbol{\pi}} - \dot{\boldsymbol{\pi}} \times \boldsymbol{\omega} - \boldsymbol{\pi} \times \dot{\boldsymbol{\omega}} - \dot{\mathbf{p}} \times \mathbf{v} - \mathbf{p} \times \dot{\mathbf{v}}, \end{cases}$$

where the linear and angular jolt co-vectors are

$$\dot{\mathbf{F}} \equiv \mathbf{M}\dot{\mathbf{v}} = [\dot{F}_1, \dot{F}_2, \dot{F}_3], \quad \dot{\mathbf{T}} \equiv \mathbf{I}\dot{\boldsymbol{\omega}} = [\dot{T}_1, \dot{T}_2, \dot{T}_3],$$

where

$$\dot{\mathbf{v}} = [\dot{v}_1, \dot{v}_2, \dot{v}_3]^t, \quad \dot{\boldsymbol{\omega}} = [\dot{\omega}_1, \dot{\omega}_2, \dot{\omega}_3]^t,$$

are linear and angular jerk vectors.

In tensor form, the $SE(3)$ -jolt reads¹⁰

$$\begin{aligned} \dot{F}_i &= \ddot{p}_i - \varepsilon_{ik}^j \dot{p}_j \omega^k - \varepsilon_{ik}^j p_j \dot{\omega}^k, \quad (i, j, k = 1, 2, 3) \\ \dot{T}_i &= \ddot{\pi}_i - \varepsilon_{ik}^j \dot{\pi}_j \omega^k - \varepsilon_{ik}^j \pi_j \dot{\omega}^k - \varepsilon_{ik}^j \dot{p}_j v^k - \varepsilon_{ik}^j p_j \dot{v}^k, \end{aligned}$$

in which the linear and angular jolt covectors are defined as:

$$\begin{aligned} \dot{\mathbf{F}} \equiv \dot{F}_i &= \mathbf{M}\dot{\mathbf{v}} \equiv M_{ij} \dot{v}^j = [\dot{F}_1, \dot{F}_2, \dot{F}_3], \\ \dot{\mathbf{T}} \equiv \dot{T}_i &= \mathbf{I}\dot{\boldsymbol{\omega}} \equiv I_{ij} \dot{\omega}^j = [\dot{T}_1, \dot{T}_2, \dot{T}_3], \end{aligned}$$

where $\dot{\mathbf{v}} = \dot{v}^i$, and $\dot{\boldsymbol{\omega}} = \dot{\omega}^i$ are linear and angular jerk vectors.

In scalar form, the $SE(3)$ -jolt expands as:

$$\begin{aligned} \text{Newton jolt} : \begin{cases} \dot{F}_1 = \ddot{p}_1 - m_2 \omega_3 \dot{v}_2 + m_3 (\omega_2 \dot{v}_3 + v_3 \dot{\omega}_2) - m_2 v_2 \dot{\omega}_3, \\ \dot{F}_2 = \ddot{p}_2 + m_1 \omega_3 \dot{v}_1 - m_3 \omega_1 \dot{v}_3 - m_3 v_3 \dot{\omega}_1 + m_1 v_1 \dot{\omega}_3, \\ \dot{F}_3 = \ddot{p}_3 - m_1 \omega_2 \dot{v}_1 + m_2 \omega_1 \dot{v}_2 - v_2 \dot{\omega}_1 - m_1 v_1 \dot{\omega}_2, \end{cases} \\ \text{Euler jolt} : \begin{cases} \dot{T}_1 = \ddot{\pi}_1 - (m_2 - m_3) (v_3 \dot{v}_2 + v_2 \dot{v}_3) - (I_2 - I_3) (\omega_3 \dot{\omega}_2 + \omega_2 \dot{\omega}_3), \\ \dot{T}_2 = \ddot{\pi}_2 + (m_1 - m_3) (v_3 \dot{v}_1 + v_1 \dot{v}_3) + (I_1 - I_3) (\omega_3 \dot{\omega}_1 + \omega_1 \dot{\omega}_3), \\ \dot{T}_3 = \ddot{\pi}_3 - (m_1 - m_2) (v_2 \dot{v}_1 + v_1 \dot{v}_2) - (I_1 - I_2) (\omega_2 \dot{\omega}_1 + \omega_1 \dot{\omega}_2). \end{cases} \end{aligned}$$

We remark here that the linear and angular momenta ($\mathbf{p}, \boldsymbol{\pi}$), forces (\mathbf{F}, \mathbf{T}) and jolts ($\dot{\mathbf{F}}, \dot{\mathbf{T}}$) are co-vectors (row vectors), while the linear and angular velocities ($\mathbf{v}, \boldsymbol{\omega}$), accelerations ($\dot{\mathbf{v}}, \dot{\boldsymbol{\omega}}$) and jerks ($\ddot{\mathbf{v}}, \ddot{\boldsymbol{\omega}}$)

are vectors (column vectors). This bio-physically means that the 'jerk' vector should not be confused with the 'jolt' co-vector. For example, the 'jerk' means shaking the head's own mass-inertia matrices (mainly in the atlanto-occipital and atlanto-axial joints), while the 'jolt' means actually hitting the head with some external mass-inertia matrices included in the 'hitting' $SE(3)$ -jolt, or hitting some external static/massive body with the head (e.g., the ground- gravitational effect, or the wall- inertial effect). Consequently, the mass-less 'jerk' vector represents a (translational+rotational) *non-collision effect* that can cause only weaker brain injuries, while the inertial 'jolt' co-vector represents a (translational+rotational) *collision effect* that can cause hard brain injuries.

For example, while driving a car, the $SE(3)$ -jerk of the head-neck system happens every time the driver brakes abruptly. On the other hand, the $SE(3)$ -jolt means actual impact to the head. Similarly, the whiplash-jerk, caused by rear-end car collisions, is like a soft version of the high pitch-jolt caused by the boxing 'upper-cut'. Also, violently shaking the head left-right in the transverse plane is like a soft version of the high yaw-jolt caused by the sidewise, or hook punch.

2.1.4. Brain's Dislocations and Disclinations Caused by the $SE(3)$ -jolt

Recall from introduction that for mild TBI, the best injury predictor is considered to be the product of brain's strain and strain rate, which is the standard isotropic viscoelastic continuum concept. To improve this standard concept, in this subsection, we consider human brain as a 3D anisotropic multipolar *Cosserat viscoelastic continuum* (see [1] and references therein), exhibiting coupled-stress-strain elastic properties. This non-standard continuum model is suitable for analyzing plastic (irreversible) deformations and fracture mechanics in multi-layered materials with microstructure (in which slips and bending of layers introduces additional degrees of freedom, non-existent in the standard continuum models).

The $SE(3)$ -jolt ($\dot{\mathbf{F}}, \dot{\mathbf{T}}$) causes two types of brain's rapid discontinuous deformations:

1. The Newton jolt $\dot{\mathbf{F}}$ can cause micro-translational *dislocations*, or discontinuities in the Cosserat translations;
2. The Euler jolt $\dot{\mathbf{T}}$ can cause micro-rotational *disclinations*, or discontinuities in the Cosserat rotations.

To precisely define brain's dislocations and disclinations, caused by the $SE(3)$ -jolt ($\dot{\mathbf{F}}, \dot{\mathbf{T}}$), we first

⁹Note that the derivative of the cross-product of two vectors follows the standard calculus product-rule: $\frac{d}{dt}(\mathbf{u} \times \mathbf{v}) = \dot{\mathbf{u}} \times \mathbf{v} + \mathbf{u} \times \dot{\mathbf{v}}$.

¹⁰In this paragraph the overdots actually denote the absolute Bianchi (covariant) time-derivative (1), so that the jolts retain the proper covector character, which would be lost if ordinary time derivatives are used. However, for the sake of simplicity and wider readability, we stick to the same overdot notation.

define the coordinate co-frame, i.e., the set of basis 1-forms $\{dx^i\}$, given in local coordinates $x^i = (x^1, x^2, x^3) = (x, y, z)$, attached to brain's center-of-mass. Then, in the coordinate co-frame $\{dx^i\}$ we introduce the following set of brain's plastic-deformation-related $SE(3)$ -based differential p -forms¹¹ (see, e.g. [7, 13]):

the *dislocation current* 1-form, $\mathbf{J} = J_i dx^i$;

the *dislocation density* 2-form, $\boldsymbol{\alpha} = \frac{1}{2}\alpha_{ij} dx^i \wedge dx^j$;

the *disclination current* 2-form, $\mathbf{S} = \frac{1}{2}S_{ij} dx^i \wedge dx^j$; and

the *disclination density* 3-form, $\mathbf{Q} = \frac{1}{3!}Q_{ijk} dx^i \wedge dx^j \wedge dx^k$,

where \wedge denotes the exterior wedge-product. According to Edelen [16, 17], these four $SE(3)$ -based differential forms satisfy the following set of continuity equations:

$$\dot{\boldsymbol{\alpha}} = -d\mathbf{J} - \mathbf{S}, \quad (6)$$

$$\dot{\mathbf{Q}} = -d\mathbf{S}, \quad (7)$$

$$d\boldsymbol{\alpha} = \mathbf{Q}, \quad (8)$$

$$d\mathbf{Q} = \mathbf{0}, \quad (9)$$

where d denotes the exterior derivative.

In components, the simplest, fourth equation (9), representing the *Bianchi identity*, can be rewritten as

¹¹Differential p -forms are totally skew-symmetric covariant tensors, defined using the exterior wedge-product and exterior derivative. The proper definition of exterior derivative d for a p -form β on a smooth manifold M , includes the *Poincaré lemma* [7, 13]: $d(d\beta) = 0$, and validates the *general Stokes formula*

$$\int_{\partial M} \beta = \int_M d\beta,$$

where M is a p -dimensional manifold with a boundary and ∂M is its $(p-1)$ -dimensional boundary, while the integrals have appropriate dimensions.

A p -form β is called *closed* if its exterior derivative is equal to zero,

$$d\beta = 0.$$

From this condition one can see that the closed form (the *kernel* of the exterior derivative operator d) is conserved quantity. Therefore, closed p -forms possess certain invariant properties, physically corresponding to the conservation laws.

A p -form β that is an exterior derivative of some $(p-1)$ -form α ,

$$\beta = d\alpha,$$

is called *exact* (the *image* of the exterior derivative operator d). By *Poincaré lemma*, exact forms prove to be closed automatically,

$$d\beta = d(d\alpha) = 0.$$

This lemma is the foundation of the de Rham cohomology theory.

$$d\mathbf{Q} = \partial_l Q_{[ijk]} dx^l \wedge dx^i \wedge dx^j \wedge dx^k = 0,$$

where $\partial_i \equiv \partial/\partial x^i$, while $\theta_{[ij\dots]}$ denotes the skew-symmetric part of $\theta_{ij\dots}$.

Similarly, the third equation (8) in components reads

$$\frac{1}{3!} \dot{Q}_{ijk} dx^i \wedge dx^j \wedge dx^k = \partial_k \alpha_{[ij]} dx^k \wedge dx^i \wedge dx^j, \quad \text{or}$$

$$Q_{ijk} = -6 \partial_k \alpha_{[ij]}.$$

The second equation (7) in components reads

$$\frac{1}{3!} \dot{Q}_{ijk} dx^i \wedge dx^j \wedge dx^k = -\partial_k S_{[ij]} dx^k \wedge dx^i \wedge dx^j, \quad \text{or}$$

$$\dot{Q}_{ijk} = 6 \partial_k S_{[ij]}.$$

Finally, the first equation (6) in components reads

$$\frac{1}{2} \dot{\alpha}_{ij} dx^i \wedge dx^j = (\partial_j J_i - \frac{1}{2} S_{ij}) dx^i \wedge dx^j, \quad \text{or}$$

$$\dot{\alpha}_{ij} = 2 \partial_j J_i - S_{ij}.$$

In words, we have:

- The 2-form equation (6) defines the time derivative $\dot{\boldsymbol{\alpha}} = \frac{1}{2} \dot{\alpha}_{ij} dx^i \wedge dx^j$ of the dislocation density $\boldsymbol{\alpha}$ as the (negative) sum of the disclination current \mathbf{S} and the curl of the dislocation current \mathbf{J} .
- The 3-form equation (7) states that the time derivative $\dot{\mathbf{Q}} = \frac{1}{3!} \dot{Q}_{ijk} dx^i \wedge dx^j \wedge dx^k$ of the disclination density \mathbf{Q} is the (negative) divergence of the disclination current \mathbf{S} .
- The 3-form equation (8) defines the disclination density \mathbf{Q} as the divergence of the dislocation density $\boldsymbol{\alpha}$, that is, \mathbf{Q} is the *exact* 3-form.
- The Bianchi identity (9) follows from equation (8) by *Poincaré lemma* and states that the disclination density \mathbf{Q} is conserved quantity, that is, \mathbf{Q} is the *closed* 3-form. Also, every 4-form in 3D space is zero.

From these equations, we can derive two important conclusions:

1. Being the derivatives of the dislocations, brain's disclinations are higher-order tensors, and thus more complex quantities, which means that they present a higher risk for the severe TBI than dislocations- an old fact which is supported by

the literature (see review of existing TBI-models given in Introduction).

2. Brain's dislocations and disclinations are mutually coupled by the underlying $SE(3)$ group, which means that we cannot separately analyze translational and rotational TBIs- a new fact which *is not* supported by the literature.

2.2. Spinal Injury Mechanics

The traditional *principal loading hypothesis* [18, 19], which describes spinal injuries in terms of spinal tension, compression, bending, and shear, is insufficient to predict and prevent the cause of the back-pain syndrome. Its underlying mechanics is simply not accurate enough.

On the other hand, to be recurrent, musculo-skeletal injury must be associated with a histological change, i.e., the modification of associated tissues within the body. However, incidences of *functional* musculoskeletal injury, e.g., lower back pain, generally shows little evidence of *structural* damage [20]. The incidence of injury is likely to be a continuum ranging from little or no evidence of structural damage through to the observable damage of muscles, joints or bones. The changes underlying functional injuries are likely to consist of torn muscle fibers, stretched ligaments, subtle erosion of joint tissues, and/or the application of pressure to nerves, all amounting to a disruption of function to varying degrees and a tendency toward spasm.

For example, in a review of experimental studies on the role of mechanical stresses in the genesis of intervertebral disk degeneration and herniation [21], the authors dismissed simple mechanical stimulations of functional vertebra as a cause of disk herniation, concluding instead that a complex mechanical stimulation combining forward and lateral bending of the spine followed by violent compression is needed to produce posterior herniation of the disk. Considering the use of models to estimate the risk of injury the authors emphasize the need to understand this complex interaction between the mechanical forces and the living body [22]. Compressive and shear loading increased significantly with exertion load, lifting velocity, and trunk asymmetry [23]. Also, it has been stated that up to two-thirds of all back injuries have been associated with trunk rotation [24]. In addition, load-lifting in awkward environment places a person at risk for low back pain and injury [25]. These risks

appear to be increased when facing up or down an inclined surface.

The above-mentioned safe spinal motions (flexion/extension, lateral flexion and rotation) *are* governed by standard Euler's rotational intervertebral dynamics coupled to Newton's micro-translational dynamics. On the other hand, the unsafe spinal events, the main cause of spinal injuries, are caused by intervertebral $SE(3)$ -jolts, the sharp and sudden, delta-(forces + torques) combined, localized both in time and in space. These localized intervertebral $SE(3)$ -jolts do not belong to the standard Newton-Euler dynamics. The only way to monitor them would be to measure *in vivo* the rate of the combined (forces + torques)- rise.

Ivancevic proposed in [2, 4] a new locally-coupled loading-rate hypothesis, which states that the main cause of both soft- and hard-tissue spinal injury is a localized Euclidean jolt, or $SE(3)$ -jolt, an impulsive loading that strikes a localized spine in several coupled degrees-of-freedom (DOF) simultaneously. To show this, based on the previously defined covariant force law, we formulate the coupled Newton-Euler dynamics of the local spinal motions and derive from it the corresponding coupled $SE(3)$ -jolt dynamics. The $SE(3)$ -jolt is the main cause of two forms of local discontinuous spinal injury: (i) hard-tissue injury of local translational dislocations; and (ii) soft-tissue injury of local rotational disclinations. Both the spinal dislocations and disclinations, as caused by the $SE(3)$ -jolt, are described using the Cosserat multipolar viscoelastic continuum model.

While we can intuitively visualize the $SE(3)$ -jolt, for the purpose of simulation we use the necessary simplified, decoupled approach (neglecting the 3D torque matrix and its coupling to the 3D force vector). Note that decoupling is a kind of linearization that prevents chaotic behavior, giving an illusion of full predictability. In this decoupled framework of reduced complexity, we define:

- The cause of hard spinal injuries (discus hernia) is a linear 3D-jolt vector hitting some intervertebral joint- the time rate-of-change of a 3D-force vector (linear jolt = mass \times linear jerk); and
- The cause of soft spinal injuries (back-pain syndrome) is an angular 3-axial jolt hitting some intervertebral joint- the time rate-of-change of a 3-axial torque (angular jolt = inertia moment \times angular jerk).

This decoupled framework has been implemented in the Human Biodynamics Engine, a world-class neuro-musculo-skeletal dynamics simulator (with 270 DOFs, the same number of equivalent muscular actuators and two-level neural reflex control), developed by the present author at Defence Science and Technology Organization, Australia. This kinematically validated human motion simulator has been described in a series of papers and books (see [26] and references therein).

As shown in [4], the mechanics of spinal (intervertebral) injury is essentially the same as the mechanics of brain injury, described in the previous subsection. In particular, we can conclude that localized spinal dislocations and disclinations are mutually coupled by the underlying $SE(3)$ -group, which means that we cannot separately analyze translational and rotational spinal injuries- a new fact which *is not* supported by the literature.

3. RIGOROUS CRASH SIMULATOR TOOLBOX FOR *Matlab*TM

A Matlab toolbox entitled *Rigorous Crash Simulator* (*RCS*) is currently under collaborative development by the Land Operations Division, Defence Science & Technology Organisation, Australia and the Centre for Intelligent Systems Research, Deakin University

[Waurm Ponds] Australia. This new toolbox is a spin-off of the Human Biodynamics Engine [26], based on two existing Matlab toolboxes: (i) third-party toolbox *DiffMan* (for solving ODEs on manifolds), by K. Engø, A. Marthinsen and H. Munthe-Kaas, and (ii) standard *Virtual Reality* (VR) toolbox for *Matlab* and Simulink.

Briefly, human spine with head and pelvis (see Figure 3), mechanically represents a chain of 27 rigid bodies, flexibly joined by 26 inter-vertebral joints. For rigorous prediction and prevention spinal injuries under various crash-impact situations, modern computational mechanics needs to be used. It is modeled as a chain of 26 Euclidean groups of motion and numerically solved by Lie-group integrators.

The *RCS* toolbox is developed around the main Lie-group integrator, called *Runge-Kutta-Munte-Kass* (RKMK) integrator (see next section).

3.1. Rigid Body Motion and ODEs on Smooth Manifolds

Recall from mechanics of brain-and-spine injury described in the previous section, that the special Euclidean group $SE(3)$ of rigid-body motions in our everyday Euclidean space \mathbb{R}^3 , is a semidirect (non-commutative) product of the rotation group $SO(3)$ and the translation group \mathbb{R}^3 . This practically means that the motion of a rigid body in a 3D space is given by a

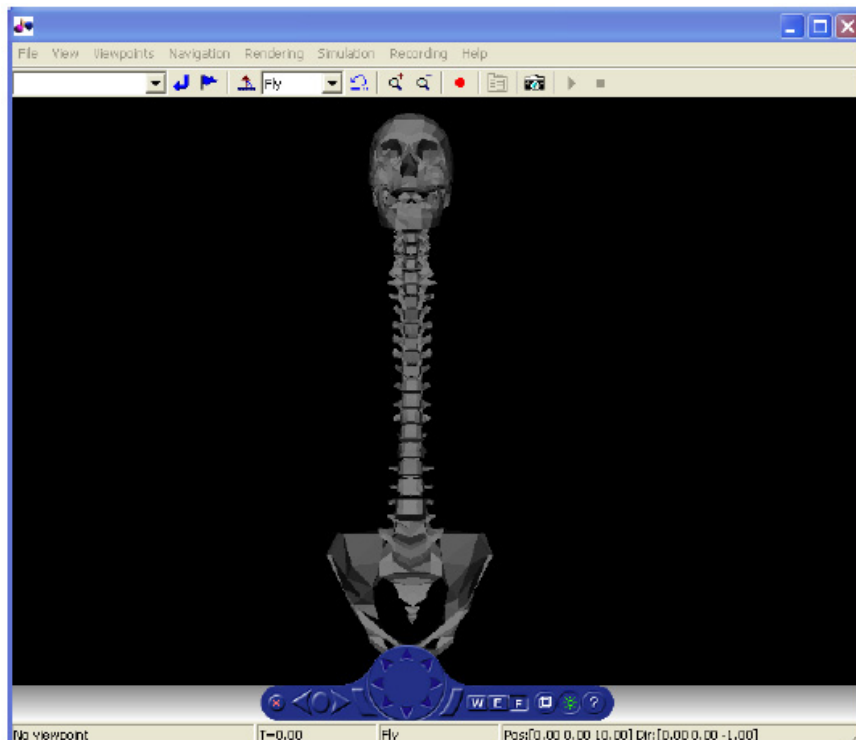


Figure 3: A 3D model of human spine implemented in the VR toolbox of *Matlab*.

pair $(R, p) \in SE(3)$ of rotation matrix R and translation vector p , such that its angular velocity (attitude) matrix ω and linear velocity vector v belong to its Lie algebra $se(3)$, that is: $(\omega, v) \in se(3) \approx \mathbb{R}^6$.

Kinematic equations of motion of a rigid body are:

$$\dot{p} = Rv, \quad \dot{R} = R\omega.$$

Kinetic energy of a rigid body has the symmetrical form:

$$E_k = \frac{1}{2} v^T M v + \frac{1}{2} \omega^T I \omega, \quad (10)$$

where (assuming uniform mass-distribution) mass and inertia matrices are diagonal:

$$M = \text{diag}\{m_1, m_2, m_3\}, \\ I = \text{diag}\{I_1, I_2, I_3\}.$$

From the kinetic energy (10), dynamical *equations of motion* follow (these are coupled Newton-Euler equations, see my injury papers for the derivation):

$$M\dot{v} = Mv \times \omega, \quad I\dot{\omega} = I\omega \times \omega + Mv \times v.$$

Finally, by including the forces f_i and torques τ_i acting on the body ($i=1, \dots, n$), with input controls $u^i = u(t)$, the dynamical-control equations become:

$$M\dot{v} = Mv \times \omega + F, \quad (\text{with } F = \sum_i f_i u^i), \quad (11)$$

$$I\dot{\omega} = I\omega \times \omega + Mv \times v + T, \quad (\text{with } T = \sum_i \tau_i u^i). \quad (12)$$

In the spinal crash-test model, the motion of the head, as well as of each individual vertebral body, is governed by the pair of vector equations (11)-(12). They are evolving on the smooth $SE(3)$ -manifold.

3.1.1. Evolving ODEs on Smooth Manifolds

To give a brief description of the computational mechanics implemented in the *RCS* toolbox, consider the following ODE (ordinary differential equation) evolving in time ($t \geq 0$) on some configuration manifold M .¹²

$$\dot{x} = F(x), \quad x(0) = x_0 \in M,$$

where $\dot{x} = dx/dt$, while $F(x) \in \chi(M)$ is the tangent *vector-field* on M passing through the points $x(t)$.

The solution of the ODE (13) is determined by its *flow* $\phi_{t,F}(x_0)$ that starts from the initial point $x(0) = x_0$, which is formally defined as:

$$x(t) = \phi_{t,F}(x_0), \quad (\text{for } t \geq 0).$$

In general, any tangent vector-field is an *infinitesimal generator* of its flow. This means that the vector-field $F(x)$ is given by the time-derivative of the flow $\phi_{t,F}(x_0)$ at the initial point:

$$F(x) = \frac{d}{dt} \phi_{t,F}(x_0) |_{t=0}.$$

The inverse of the time-derivative of the flow is something that plays the role of the time-integral, which is the *exponential map*, a nonlinear generalization of the matrix exponential. So, the flow $\phi_{t,F}$ is given by the exponential map of (tF) :

$$\phi_{t,F} = \exp(tF).$$

In the special case of the linear ODE defined by some matrix A :

$$\dot{x} = Ax, \quad \text{we have}$$

$$\phi_{t,A}(x) = \exp(tA)x_0 \quad (14)$$

with the standard *matrix exponential*:

$$\exp(tA) = \sum_{n=0}^{\infty} \frac{1}{n!} t^n A^n.$$

In the case of linear ODEs, solved by the matrix exponentials, we can see that their flows do not commute: going first along the flow $\phi_{t,A}$ and then along some other flow $\phi_{t,B}$ is different from going first along the flow $\phi_{t,B}$ and then along the flow $\phi_{t,A}$. This is because matrix multiplication is not commutative, so it yields the *commutator*:

$$[A, B] = AB - BA \neq 0.$$

This non-commutativity of flows is even more significant in a general case of nonlinear ODEs. Let us start from some point x_0 on the manifold M , and flow from x_0 first along $\phi_{t,F} = \exp(tF)$ and then along some other flow $\phi_{t,G} = \exp(tG)$, so that we come to some point x_1 . If we now reverse the order of flows and starting from the same point x_0 we flow first along $\phi_{t,G}$

¹²For example, $M = SE(3)$, the configuration manifold of a rigid body.

and then along $\phi_{t,F}$ - we will in general arrive at a different point $x_2 \neq x_1$. In terms of exponential maps this non-commutativity of flows can be written as:

$$\exp(sF) \circ \exp(tG) \circ \exp(-sF) \circ \exp(-tG) \neq 0.$$

If the flows do not commute, then their vector-fields do not commute either. This statement is defined by the commutator $[F,G] \neq 0$ called the *Lie bracket* of vector-fields F and G , which has the following three properties:

$$\begin{aligned} [F,G] &= -[G,F], \\ [F+G,H] &= [F,H] + [G,H], \\ 0 &= [F,[G,H]] + [G,[H,F]] + [H,[F,G]], \end{aligned}$$

called anti-symmetry, bilinearity and Jacobi identity, respectively. The set of all tangent vector-fields $\chi(M)$ on the manifold M now (with the Lie bracket) becomes the *Lie algebra*.

3.1.2. Runge-Kutta-Munte-Kass Family of Lie-Group Integrators

The *RCS* toolbox is developed around the main Lie-group integrator, called Runge-Kutta-Munte-Kass (RKMK) integrator [27, 28], which combines standard Runge-Kutta family with Lie-group integration methods developed by A. Iserles (for a recent review, see [32]) and H. Munthe-Kaas [29-31].

ODEs are solved in DiffMan using the following general 5-step procedure:¹³

1. Construct an initial domain object y in a homogeneous space;
2. Construct a vector-field object vf over the domain object y ; DiffMan finds numerically the integral curve of this vector-field through the initial domain object;
3. Construct a time stepper object ts , which determines the numerical method used to advance the numerical solution along the integral line; it consists of two parts: coordinate and method;
4. Construct a flow object f , which is defined by the vector-field object; and
5. Solve the ODE by the flow object which is done by evaluating the flow object at the initial domain object, start time, end time, and step size.

3.2. Computational Newton-Euler Dynamics

3.2.1. First-Order (Velocities) Equations of Motion

Standard description of Newton-Euler dynamics starts with the first-order equations of motion in terms of translational and rotational velocities:¹⁴

$$\text{Newton : } \begin{cases} \dot{p}_1(t) \equiv m_1 v_1(t) = F_1(t) - m_3 v_3(t) \omega_2(t) + m_2 v_2(t) \omega_3(t), \\ \dot{p}_2(t) \equiv m_2 v_2(t) = F_2(t) - m_3 v_3(t) \omega_1(t) - m_1 v_1(t) \omega_3(t), \\ \dot{p}_3(t) \equiv m_3 v_3(t) = F_3(t) - m_2 v_2(t) \omega_1(t) + m_1 v_1(t) \omega_2(t). \end{cases}$$

$$\text{Euler : } \begin{cases} \dot{\pi}_1(t) \equiv J_1 \omega_1(t) = T_1(t) + (J_2 - J_3) \omega_2(t) \omega_3(t) + (m_2 - m_3) v_2(t) v_3(t), \\ \dot{\pi}_2(t) \equiv J_2 \omega_2(t) = T_2(t) + (J_3 - J_1) \omega_1(t) \omega_3(t) + (m_3 - m_1) v_1(t) v_3(t), \\ \dot{\pi}_3(t) \equiv J_3 \omega_3(t) = T_3(t) + (J_1 - J_2) \omega_1(t) \omega_2(t) + (m_1 - m_2) v_1(t) v_2(t). \end{cases}$$

Numerical solution of these equations (for some initial conditions) gives translational and rotational velocities ($v_i(t)$ and $\omega_i(t)$, $i=1,2,3$). However, to be able to actually see the body motion in a virtual 3D environment, we need to evaluate these equations into the second-order equations in terms of translations (displacements x_i) and rotations (Euler angles θ_i).

3.2.2. Second-Order (Coordinates) Equations of Motion

The above standard first-order Newton-Euler velocity equations are expanded/evaluated into the following coordinate equations of motion:

$$\text{Newton : } \begin{cases} \dot{p}_1(t) \equiv m_1 \ddot{x}_1(t) = -m_3 \dot{x}_3(t) \dot{\theta}_2(t) + m_2 \dot{x}_2(t) \dot{\theta}_3(t) - b_1 \dot{x}_1(t) - k_1 x_1(t), \\ \dot{p}_2(t) \equiv m_2 \ddot{x}_2(t) = -m_3 \dot{x}_3(t) \dot{\theta}_1(t) - m_1 \dot{x}_1(t) \dot{\theta}_3(t) - b_2 \dot{x}_2(t) - k_2 x_2(t), \\ \dot{p}_3(t) \equiv m_3 \ddot{x}_3(t) = -m_2 \dot{x}_2(t) \dot{\theta}_1(t) + m_1 \dot{x}_1(t) \dot{\theta}_2(t) - b_3 \dot{x}_3(t) - k_3 x_3(t). \end{cases}$$

$$\text{Euler : } \begin{cases} \dot{\pi}_1(t) \equiv J_1 \ddot{\theta}_1(t) = (J_2 - J_3) \dot{\theta}_2(t) \dot{\theta}_3(t) + (m_2 - m_3) \dot{x}_2(t) \dot{x}_3(t) - B_1 \dot{\theta}_1(t) - K_1 \theta_1(t), \\ \dot{\pi}_2(t) \equiv J_2 \ddot{\theta}_2(t) = (J_3 - J_1) \dot{\theta}_1(t) \dot{\theta}_3(t) + (m_3 - m_1) \dot{x}_1(t) \dot{x}_3(t) - B_2 \dot{\theta}_2(t) - K_2 \theta_2(t), \\ \dot{\pi}_3(t) \equiv J_3 \ddot{\theta}_3(t) = (J_1 - J_2) \dot{\theta}_1(t) \dot{\theta}_2(t) + (m_1 - m_2) \dot{x}_1(t) \dot{x}_2(t) - B_3 \dot{\theta}_3(t) - K_3 \theta_3(t). \end{cases}$$

For simplicity, in these evaluated 2nd order equations of motion, forces $F_i(t)$ are replaced by springs $k_i x_i(t)$ and dampers $b_i \dot{x}_i(t)$; and similarly for rotations, instead of torques $T_i(t)$ we have angular springs $K_i \theta_i(t)$ and angular dampers $B_i \dot{\theta}_i(t)$.

3.2.3. Computational form of Newton-Euler Equations of Rigid Motions Newton-Euler Acceleration ODEs

Newton-Euler acceleration ODEs are defined as:

¹³For technical details with worked examples, see [27, 28].

¹⁴ \equiv means ekvivalent, whatever is left from it is not part of the equations to be solved.

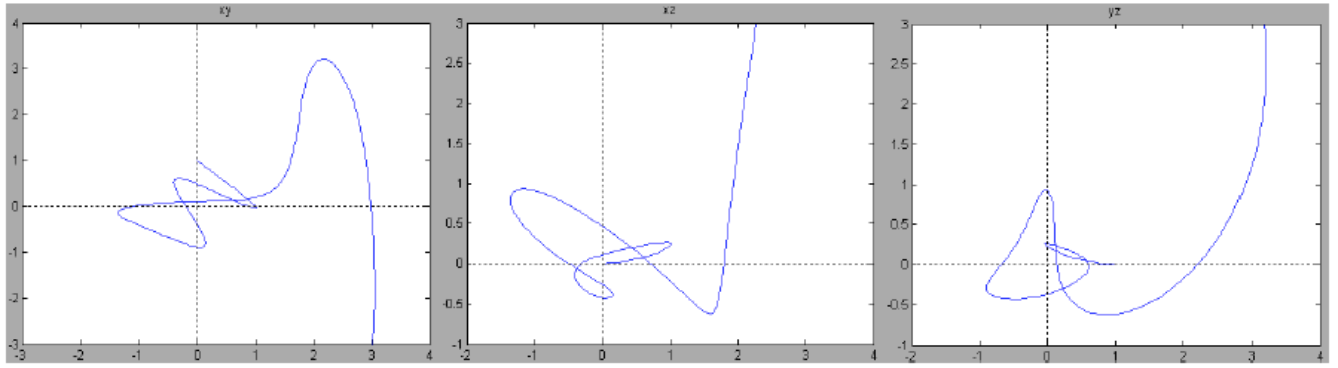


Figure 4: Test problem: solution of the 2nd-order Lorenz-like ODEs in Matlab, using the RKMK integrator. The phase plots are identical to those calculated by Mathematica's integrator NDSolve.

$$\text{Newton : } \begin{cases} \ddot{x}_1(t) = [-m_3\dot{x}_3(t)\dot{\theta}_2(t) + m_2\dot{x}_2(t)\dot{\theta}_3(t) - b_1\dot{x}_1(t) - k_1x_1(t)] / m_1, \\ \ddot{x}_2(t) = [-m_3\dot{x}_3(t)\dot{\theta}_1(t) - m_1\dot{x}_1(t)\dot{\theta}_3(t) - b_2\dot{x}_2(t) - k_2x_2(t)] / m_2, \\ \ddot{x}_3(t) = [-m_2\dot{x}_2(t)\dot{\theta}_1(t) + m_1\dot{x}_1(t)\dot{\theta}_2(t) - b_3\dot{x}_3(t) - k_3x_3(t)] / m_3, \end{cases}$$

$$\text{Euler : } \begin{cases} \ddot{\theta}_1(t) = [(J_2 - J_3)\dot{\theta}_2(t)\dot{\theta}_3(t) + (m_2 - m_3)\dot{x}_2(t)\dot{x}_3(t) - B_1\dot{\theta}_1(t) - K_1\theta_1(t)] / J_1, \\ \ddot{\theta}_2(t) = [(J_3 - J_1)\dot{\theta}_1(t)\dot{\theta}_3(t) + (m_3 - m_1)\dot{x}_1(t)\dot{x}_3(t) - B_2\dot{\theta}_2(t) - K_2\theta_2(t)] / J_2, \\ \ddot{\theta}_3(t) = [(J_1 - J_2)\dot{\theta}_1(t)\dot{\theta}_2(t) + (m_1 - m_2)\dot{x}_1(t)\dot{x}_2(t) - B_3\dot{\theta}_3(t) - K_3\theta_3(t)] / J_3, \end{cases}$$

Full set of first-order ODEs suitable for numerical integration.

The following set of 12 first-order ODEs has been implemented in the *RCS* toolbox for simulating a single intervertebral joint:

$$\begin{aligned} \dot{x}_1(t) &= v_1(t), \\ \dot{v}_1(t) &= [-m_3\dot{x}_3(t)\dot{\theta}_2(t) + m_2\dot{x}_2(t)\dot{\theta}_3(t) - b_1\dot{x}_1(t) - k_1x_1(t)] / m_1, \\ \dot{x}_2(t) &= v_2(t), \\ \dot{v}_2(t) &= [-m_3\dot{x}_3(t)\dot{\theta}_1(t) - m_1\dot{x}_1(t)\dot{\theta}_3(t) - b_2\dot{x}_2(t) - k_2x_2(t)] / m_2, \\ \dot{x}_3(t) &= v_3(t), \\ \dot{v}_3(t) &= [-m_2\dot{x}_2(t)\dot{\theta}_1(t) + m_1\dot{x}_1(t)\dot{\theta}_2(t) - b_3\dot{x}_3(t) - k_3x_3(t)] / m_3, \\ \dot{\theta}_1(t) &= \omega_1(t), \\ \dot{\omega}_1(t) &= [(J_2 - J_3)\dot{\theta}_2(t)\dot{\theta}_3(t) + (m_2 - m_3)\dot{x}_2(t)\dot{x}_3(t) - B_1\dot{\theta}_1(t) - K_1\theta_1(t)] / J_1, \\ \dot{\theta}_2(t) &= \omega_2(t), \\ \dot{\omega}_2(t) &= [(J_3 - J_1)\dot{\theta}_1(t)\dot{\theta}_3(t) + (m_3 - m_1)\dot{x}_1(t)\dot{x}_3(t) - B_2\dot{\theta}_2(t) - K_2\theta_2(t)] / J_2, \\ \dot{\theta}_3(t) &= \omega_3(t), \\ \dot{\omega}_3(t) &= [(J_1 - J_2)\dot{\theta}_1(t)\dot{\theta}_2(t) + (m_1 - m_2)\dot{x}_1(t)\dot{x}_2(t) - B_3\dot{\theta}_3(t) - K_3\theta_3(t)] / J_3, \end{aligned} \quad (15)$$

init. conds : $x_i(0) = a_i$, $\dot{x}_i(0) = c_i$, $\theta_i(0) = d_i$, $\dot{\theta}_i(0) = e_i$, (for $i = 1, 2, 3$).

The ODEs (15) have been solved using the RKMK integrator, as follows.

3.2.4. Matlab/DiffMan implementation

Testing the RKMK Integrator.

For testing the RKMK integrator, we implemented three second-order Lorenz-like ODEs, rewritten as six coupled first-order ODEs. In *Mathematica*TM, these equations are implemented as:

$$\begin{cases} x'(t) = v_1(t), & v_1'(t) = y(t) - x(t), \\ y'(t) = v_2(t), & v_2'(t) = x(t)(-z(t)) + x(t) - y(t), \\ z'(t) = v_3(t), & v_3'(t) = x(t)y(t) - z(t), \\ x(0) = z(0) = 0.001, & y(0) = 1, \\ v_1(0) = v_2(0) = v_3(0) = 0.01. \end{cases}$$

and solved using the *NDSolve* integrator for 15 sec.

In *DiffMan* these ODEs are implemented in the following m-function:¹⁵

function [la] = vfexShady2Lorenz(t,y)

```
la = liealgebra(y);
ydat = getdata(y);
dat = [ 0 0 0 -1 1 0;
        0 0 0 1 -1 -ydat(4);
        0 0 0 0 ydat(4) - 1;
        1 0 0 0 0 0;
        0 1 0 0 0 0;
        0 0 1 0 0 0; ];
```

```
setdata(la,dat);
```

```
return;
```

The phase plots of this test problem for 15 sec are shown in Figure 4.

DiffMan implementation of the system (15).

Matlab/DiffMan implementation of the system (15), using the RKMK integrator, is given by the following two m-function:

¹⁵More precisely, to implement any particular ODE-system in *DiffMan*, two m-functions are required. We are showing here only the first function (in which the ODEs are implemented), while we are skipping the second function (which calls the first one), because it is too long and out of scope of this paper.

```

function [la] = vfexShady2(t,y)
la = liealgebra(y);
ydat = getdata(y);
global k1 k2 k3 b1 b2 b3 B1 B2 B3 K1 K2 K3 m1 m2
m3 J1 J2 J3
dat = [0 1 0 0 0 0 0 0 0 0 0 0];
-k1-b1 0 0 0 0 0 0 0 0-m3*ydat(6) 0 m2*ydat(4);
0 0 0 1 0 0 0 0 0 0 0 0;
0 0-k2-b2 0 0 0 0-m3*ydat(6) 0 0 0-m1*ydat(2);
0 0 0 0 1 0 0 0 0 0 0 0;
0 0 0 0-k3-b3 0-m2*ydat(4) 0 m1*ydat(2) 0 0;
0 0 0 0 0 0 1 0 0 0 0 0;
0 0 0 0 0 (m2-m3)*ydat(4)-K1-B1 0 0 0 (J2-
J3)*ydat(10);
0 0 0 0 0 0 0 0 0 1 0 0;
0 0 0 0 0 (m3-m1)*ydat(2) 0 0-K2-B2 0 (J3-J1)*ydat(8);
0 0 0 0 0 0 0 0 0 0 0 1;
0 0 0 (m1-m2)*ydat(2) 0 0 0 0 0 (J1-J2)*ydat(8)-K3-
B3];
setdata(la,dat);
return;

```

Initial modeling of external impact forces for the crash simulation.

To simulate the action of an impact force on the single intervertebral joint, a 'soft form of' the *impulse Dirac delta function* term with amplitude A has been modeled by:

$$F(t) = A \operatorname{sech}(At - A/2),$$

and added to translational Newtonian accelerations only. Due to translational/rotational coupling between Newton's and Euler's equations within the $SE(3)$ -group dynamics, this translational impact force should cause both macroscopic angular change and microscopic displacement change within the intervertebral joint. This type of impact forces with amplitudes in the range 20g-100g are used to model road-vehicle crashes, while the amplitudes in the range 100g-400g are used to model land-mine related crashes and helicopter hard landings. In addition, for modeling effects of riding an operational watercraft with the speed of 20-30 knots on the high seas with waves of 2m-3m high, the following sinus forces with frequency φ are used:

$$F(t) = A \sin(\varphi t).$$

To test RKMK integrator on the impact forces (16)-(17) the following two versions of the forced Van der Pol oscillator (with parameters a, b, w):

$$\begin{aligned} \text{sech: } \ddot{x}(t) &= A \operatorname{sech}(At - A/2) - a \left[1 - 4bx(t)^2 \right] \dot{x}(t) + w^2 x(t), \\ \text{sin: } \ddot{x}(t) &= A \sin(\varphi t) - a \left[1 - 4bx(t)^2 \right] \dot{x}(t) + w^2 x(t), \end{aligned}$$

for the simulation with near-zero initial conditions, have been implemented in the following two m-functions, respectively:

```

function [la] = vfexVdPolSech(t,y)
la = liealgebra(y);
ydat = getdata(y);
a=1.5; b=5; w=2; A=20;
dat=[ 0 1 ;
-w*w+A*sech(A*t-A/2)/ydat(1) a*(1-
4*b*ydat(1)*ydat(1))];
setdata(la,dat);
return;

function [la] = vfexVdPolSin(t,y)
la = liealgebra(y);
ydat = getdata(y);
a=1.5;b=5;w=2;A=20;fr=3;
dat=[ 0 1 ;
-w*w+A*sin(fr*t)/ydat(1) a*(1-4*b*ydat(1)*ydat(1))];
setdata(la,dat);
return;

```

Full set of the forced first-order ODEs for a single joint crash dynamics.

After successful tasting of the forced Van der Pol oscillators (18) against Mathematica's integrator NDSolve using the above m-functions, the following set of 12 first-order $SE(3)$ -ODEs has been implemented in the *RCS* toolbox for simulating an impact force action on a single intervertebral joint:

$$\begin{aligned} \dot{x}_1(t) &= v_1(t), \\ v_1(t) &= [-m_3 \dot{x}_3(t) \dot{\theta}_2(t) + m_2 \dot{x}_2(t) \dot{\theta}_3(t) - b_1 \dot{x}_1(t) - k_1 x_1(t) + A_1 \operatorname{sech}(A_1 t - A_1/2)] / m_1, \\ \dot{x}_2(t) &= v_2(t), \\ v_2(t) &= [-m_3 \dot{x}_3(t) \dot{\theta}_1(t) - m_1 \dot{x}_1(t) \dot{\theta}_3(t) - b_2 \dot{x}_2(t) - k_2 x_2(t) + A_2 \operatorname{sech}(A_2 t - A_2/2)] / m_2, \\ \dot{x}_3(t) &= v_3(t), \\ v_3(t) &= [-m_2 \dot{x}_2(t) \dot{\theta}_1(t) + m_1 \dot{x}_1(t) \dot{\theta}_2(t) - b_3 \dot{x}_3(t) - k_3 x_3(t) + A_3 \operatorname{sech}(A_3 t - A_3/2)] / m_3, \\ \dot{\theta}_1(t) &= \omega_1(t), \\ \omega_1(t) &= [(J_2 - J_3) \dot{\theta}_2(t) \dot{\theta}_3(t) + (m_2 - m_3) \dot{x}_2(t) \dot{x}_3(t) - B_1 \dot{\theta}_1(t) - K_1 \theta_1(t)] / J_1, \\ \dot{\theta}_2(t) &= \omega_2(t), \\ \omega_2(t) &= [(J_3 - J_1) \dot{\theta}_1(t) \dot{\theta}_3(t) + (m_3 - m_1) \dot{x}_1(t) \dot{x}_3(t) - B_2 \dot{\theta}_2(t) - K_2 \theta_2(t)] / J_2, \\ \dot{\theta}_3(t) &= \omega_3(t), \\ \omega_3(t) &= [(J_1 - J_2) \dot{\theta}_1(t) \dot{\theta}_2(t) + (m_1 - m_2) \dot{x}_1(t) \dot{x}_2(t) - B_3 \dot{\theta}_3(t) - K_3 \theta_3(t)] / J_3, \\ \text{i.c.: } x_i(0) &= a_i, \quad \dot{x}_i(0) = c_i, \quad \theta_i(0) = d_i, \quad \dot{\theta}_i(0) = e_i, \quad (\text{for } i = 1, 2, 3). \end{aligned} \quad (19)$$

DiffMan implementation of the full set of the forced first-order ODEs for a single joint crash dynamics.

The full set of forced $SE(3)$ -ODEs (19) has been implemented in the following m-function:

```
function [la] = vfexShady4(t,y)
la = liealgebra(y);
ydat = getdata(y);
global k1 k2 k3 b1 b2 b3 B1 B2 B3 K1 K2 K3 m1 m2
m3 J1 J2 J3
global A1 A2 A3 A4 A5 A6
val1=A1*sech(A1*t-A1/2);
val2=A2*sech(A2*t-A2/2);
val3=A3*sech(A3*t-A3/2);
dat = [0 1 0 0 0 0 0 0 0 0 0 0;
(-k1+val1/ydat(2))-b1 0 0 0 0 0 0 0 0-m3*ydat(6) 0
m2*ydat(4);
0 0 0 1 0 0 0 0 0 0 0 0;
val2/ydat(4) 0-k2-b2 0 0 0-m3*ydat(6) 0 0 0-
m1*ydat(2);
0 0 0 0 0 1 0 0 0 0 0 0;
val3/ydat(6) 0 0 0-k3-b3 0-m2*ydat(4) 0 m1*ydat(2) 0
0;
0 0 0 0 0 0 1 0 0 0 0 0;
0 0 0 0 0 (m2-m3)*ydat(4)-K1-B1 0 0 0 (J2-
J3)*ydat(10);
0 0 0 0 0 0 0 0 0 1 0 0;
0 0 0 0 0 (m3-m1)*ydat(2) 0 0-K2-B2 0 (J3-J1)*ydat(8);
0 0 0 0 0 0 0 0 0 0 0 1;
0 0 0 (m1-m2)*ydat(2) 0 0 0 0 0 (J1-J2)*ydat(8)-K3-
B3];
setdata(la,dat);
return;
```

3.3. Full Spine Crash Simulator

The full spine crash simulator, as implemented in the *RCS* toolbox, figures the forced $SE(3)$ -equations of motion (19) at each spinal (intervertebral) joint independently. This *dynamical decoupling along the spine* is the only way to deal with the shear dimensionality of our problem: seven $SE(3)$ -joints for the neck only (cervical spine) and 26 $SE(3)$ -joints for the full spine. To compensate for this dynamical decoupling along the spine, at the same time we are inertially re-coupling all the joints along the spine: in the first joint (above the C1) the only mass is the head; in the second joint (above the C2) we have two masses: the head and C1; in the third joint (above C3) we have three masses: head + C1 + C2, etc. Regarding simulating various crashes, in the *RCS* toolbox, the so-called 'generic crash' is represented by a 3D force-vector which hits somewhere along the spine, at one only vertebral joint, so this force vector has 3 components:

$$F_{\text{crash}}(t) = \begin{bmatrix} A_1 \text{sech}(A_1 t - A_1 / 2), A_2 \\ \text{sech}(A_2 t - A_2 / 2), A_3 \text{sech}(A_3 t - A_3 / 2) \end{bmatrix}.$$

The full spine crash simulator has been implemented in the form of the following vector of 26 $SE(3)$ -equations of motion (with the joint-labeling superscript index $j=1,\dots,26$):

$$\begin{aligned} \dot{x}_1^j(t) &= v_1^j(t), \\ \dot{v}_1^j(t) &= [-m_3^j \dot{x}_2^j(t) \dot{\theta}_2^j(t) + m_2^j \dot{x}_2^j(t) \dot{\theta}_3^j(t) - b_1^j \dot{x}_1^j(t) - k_1^j x_1^j(t) + A_1^j \text{sech}(A_1^j t - A_1^j / 2)] / m_1^j, \\ \dot{x}_2^j(t) &= v_2^j(t), \\ \dot{v}_2^j(t) &= [-m_3^j \dot{x}_3^j(t) \dot{\theta}_1^j(t) - m_1^j \dot{x}_1^j(t) \dot{\theta}_3^j(t) - b_2^j \dot{x}_2^j(t) - k_2^j x_2^j(t) + A_2^j \text{sech}(A_2^j t - A_2^j / 2)] / m_2^j, \\ \dot{x}_3^j(t) &= v_3^j(t), \\ \dot{v}_3^j(t) &= [-m_2^j \dot{x}_3^j(t) \dot{\theta}_1^j(t) + m_1^j \dot{x}_1^j(t) \dot{\theta}_2^j(t) - b_3^j \dot{x}_3^j(t) - k_3^j x_3^j(t) + A_3^j \text{sech}(A_3^j t - A_3^j / 2)] / m_3^j, \\ \dot{\theta}_1^j(t) &= \omega_1^j(t), \\ \dot{\omega}_1^j(t) &= [(J_2^j - J_3^j) \dot{\theta}_2^j(t) \dot{\theta}_3^j(t) + (m_2^j - m_3^j) \dot{x}_2^j(t) \dot{x}_3^j(t) - B_1^j \dot{\theta}_1^j(t) - K_1^j \theta_1^j(t)] / J_1^j, \\ \dot{\theta}_2^j(t) &= \omega_2^j(t), \\ \dot{\omega}_2^j(t) &= [(J_3^j - J_1^j) \dot{\theta}_1^j(t) \dot{\theta}_3^j(t) + (m_3^j - m_1^j) \dot{x}_1^j(t) \dot{x}_3^j(t) - B_2^j \dot{\theta}_2^j(t) - K_2^j \theta_2^j(t)] / J_2^j, \\ \dot{\theta}_3^j(t) &= \omega_3^j(t), \\ \dot{\omega}_3^j(t) &= [(J_1^j - J_2^j) \dot{\theta}_1^j(t) \dot{\theta}_2^j(t) + (m_1^j - m_2^j) \dot{x}_1^j(t) \dot{x}_2^j(t) - B_3^j \dot{\theta}_3^j(t) - K_3^j \theta_3^j(t)] / J_3^j, \\ \text{i.c.: } x_1^j(0) &= a_1^j, \quad \dot{x}_1^j(0) = c_1^j, \quad \theta_1^j(0) = d_1^j, \quad \dot{\theta}_1^j(0) = e_1^j, \quad (\text{for } i=1,2,3). \end{aligned}$$

In the full spine $SE(3)$ -crash model (20), all crash amplitudes A_i^j (for $i=1,\dots,3; j=1,\dots,26$) are assumed zero, unless the impact joint has been selected with its 3 amplitudes only (e.g., A_i^7 - for the C7 cervical intervertebral joint).

In the Matlab implementation of (20) in the *RCS* toolbox (see Figure 5), the external forces are applied to each rigid body in the spinal system: all vertebrae as well as the head and the pelvis. To propagate the force effect along the spine we make use of both graphical and numerical vertebral inter-dependency. In the graphical part, the whole spine is modeled as a tree structure. All vertebrae are children to the pelvis and they are also connected to the head (which is the grandchild). So, the transformation of each spinal part affects all its children. In the numerical part, the transform propagation is modeled as a mass-propagation. Here, the mass of each spinal part is equal to the accumulated mass of all its children plus its own mass.

DiffMan implementation of the full spine crash simulator (20).

The full set of forced $SE(3)$ -ODEs (20) has been implemented, for each spinal joint independently, in the following m-function:

```
function [la] = vfexShady5(t,y)
la = liealgebra(y);
ydat = getdata(y);
global k1 k2 k3 b1 b2 b3 B1 B2 B3 K1 K2 K3 m1 m2
m3 J1 J2 J3
```

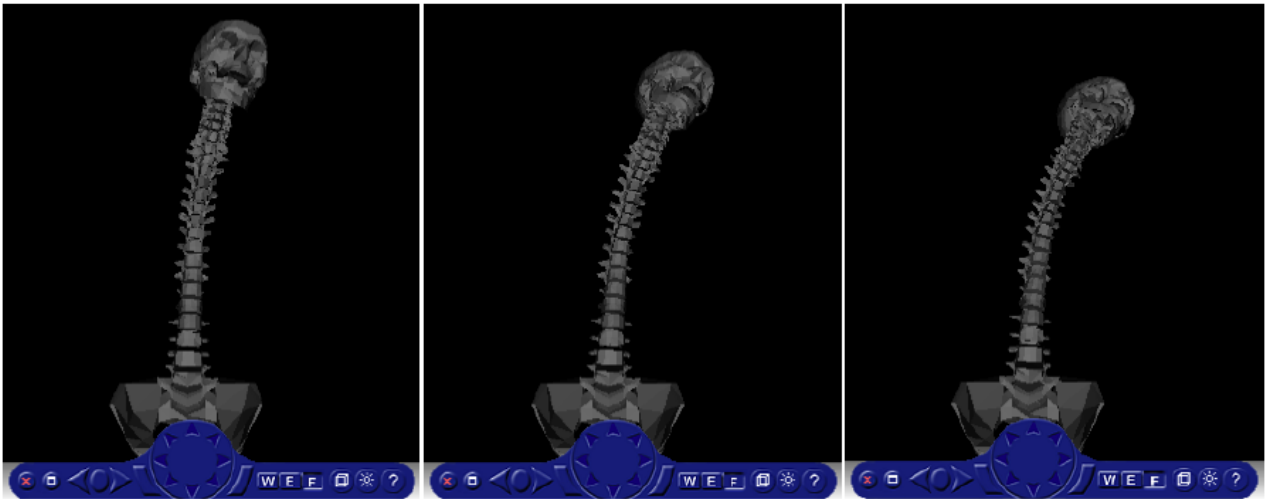



Figure 5: RCS toolbox at work: simulating a boxing punch (left hook) in the head.

```

global A1 A2 A3 A4 A5 A6
global prev_data
%x
if ~isWithin(ydat(1),-0.001,0.001)
ydat(1)=clip(ydat(1),-0.01,0.01);
ydat(2)=clip(ydat(2),10,10);
end
%y
if ~isWithin(ydat(3),-0.001,0.001)
ydat(3)=clip(ydat(3),-0.01,0.01);
ydat(4)=clip(ydat(4),10,10);
end
%z
if ~isWithin(ydat(5),-0.001,0.001)
ydat(5)=clip(ydat(5),-0.01,0.01);
ydat(6)=clip(ydat(6),10,10);
end
%th1
if ~isWithin(ydat(7),-0.01,0.01)
ydat(7)=clip(ydat(7),-0.01,0.01);
ydat(8)=clip(ydat(8),100,100);
end
%th2
if ~isWithin(ydat(9),-0.01,0.01)
ydat(9)=clip(ydat(9),-0.01,0.01);
ydat(10)=clip(ydat(10),100,100);
end
%th3
if ~isWithin(ydat(11),-0.01,0.01)
ydat(11)=clip(ydat(11),-0.01,0.01);
ydat(12)=clip(ydat(12),100,100);
end
val1=A1*sech(A1*t-A1/2);
val2=A2*sech(A2*t-A2/2);

```

```

val3=A3*sech(A3*t-A3/2);
dat = [0 1 0 0 0 0 0 0 0 0 0;
(-k1+val1/ydat(2))-b1 0 0 0 0 0 0 0 0-m3*ydat(6) 0
m2*ydat(4);
0 0 0 1 0 0 0 0 0 0 0;
val2/ydat(4) 0-k2-b2 0 0 0-m3*ydat(6) 0 0 0-m
m1*ydat(2);
0 0 0 0 1 0 0 0 0 0 0;
val3/ydat(6) 0 0 0-k3-b3 0-m2*ydat(4) 0 m1*ydat(2) 0 0;
0 0 0 0 0 0 1 0 0 0 0;
0 0 0 0 0 0 (m2-m3)*ydat(4)-K1-B1 0 0 0 (J2-
J3)*ydat(10);
0 0 0 0 0 0 0 0 1 0 0;
0 0 0 0 0 (m3-m1)*ydat(2) 0 0-K2-B2 0 (J3-J1)*ydat(8);
0 0 0 0 0 0 0 0 0 0 1;
0 0 0 (m1-m2)*ydat(2) 0 0 0 0 0 (J1-J2)*ydat(8)-K3-B3];
setdata(la,dat);
return;

```

3.4. Road-Vehicle Crash Simulation

Several crashes are implemented in the *RCS* toolbox, including road-vehicle crash, ejection seat and land-mine crash. In particular, Figure 6 shows the basic implementation of the road-vehicle crash. Note that, about 1 sec after the crash, the head moves back purely due to spinal elasticity. This particular simulated crash could cause severe TBI if the distance from the head and the steering wheel (or some other frontal part of cabin) is shorter than the movement amplitude. If the distance is safe, only a mild loss of consciousness for a few minutes could be expected, together with the strain in the cervical spine (neck).

4. CONCLUSION AND FUTURE CONSIDERATIONS

We have presented the unique mechanics of traumatic brain-and-spine injury based on the new

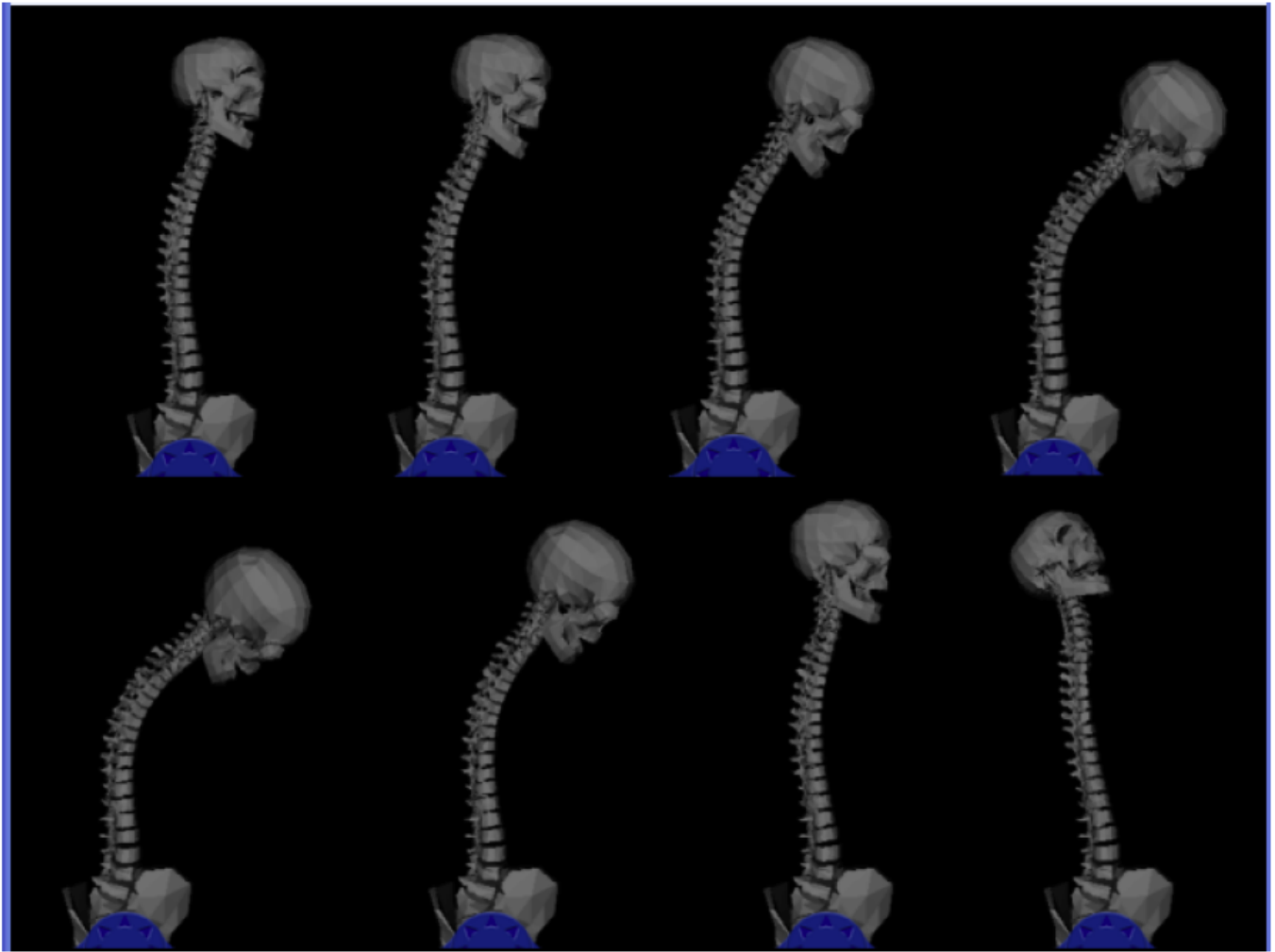


Figure 6: Road-vehicle crash simulation in the *RCS* toolbox: the sequence of 8 snapshots (starting with top-left and finishing with bottom-right) simulates the frontal (head-on) crash at the combined speed of two cars of about 80 km/h with the proper seat-belt on.

coupled loading-rate hypothesis, which states that the main cause of all mechanical human injuries is the Euclidean jolt, an impulsive loading that strikes head and spine (or any other part of the human body)- in several coupled degrees-of-freedom simultaneously, which causes two basic forms of brain and spinal injuries: (i) localized translational dislocations; and (ii) localized rotational disclinations. This model-theory of traumatic brain-and-spine injury is supported by the Rigorous Crash Simulator toolbox for *Matlab*, to be used for modeling high-impact crashes which can lead to both brain and spinal injuries. An example of road-vehicle crash is included.

Future research is planned in the following two parallel directions:

- (i) Extending the model to cover the whole human musculo-skeletal system; and

- (ii) Validation of the model against the experimental data, using both optical kinematic 'Vicon' system and mechanical 'Xsens' system (including 3D accelerometers, gyros and magnetometers). The expected outcome of the future research would be validated whole body biomechanical simulator.

ACKNOWLEDGEMENTS

The authors are grateful for the financial help received from both the Defence Science & Technology Organisation and the Deakin University, Centre for Intelligent Systems Research.

REFERENCES

- [1] Ivancevic VG. New mechanics of traumatic brain injury. *Cogn Neurodyn* 2009; 3: 281-293. <http://dx.doi.org/10.1007/s11571-008-9070-0>

- [2] Ivancevic VG. New mechanics of spinal injury. IJAM 2009; 1(2): 387-401.
- [3] Ivancevic VG. New mechanics of generic musculo-skeletal injury. BRL 2009; 4(3): 273-287
- [4] Ivancevic VG. A unique cause of traumatic brain injury and all neuro-musculo-skeletal injuries. Brain Res J 2010; 3(2): 1935-2875.
- [5] Ivancevic VG, Ivancevic TT. Natural Biodynamics. World Scientific, Series: Mathematical Biology, Singapore 2006.
- [6] Ivancevic V, Ivancevic T. Human-Like Biomechanics. Springer, Dordrecht 2006.
- [7] Ivancevic VG, Ivancevic TT. Geometrical Dynamics of Complex Systems: A Unified Modelling Approach to Physics Control Biomechanics Neurodynamics and Psycho-Socio-Economical Dynamics. Springer, Dordrecht 2006. <http://dx.doi.org/10.1007/1-4020-4545-X>
- [8] Chen Z, Cao J, Cao Y, Zhang Y, Gu F, Zhu G, Hong Z, Wang B, Cichocki A. An empirical EEG analysis in brain death diagnosis for adults. Cogn Neurodyn 2008; 2: 257-271. <http://dx.doi.org/10.1007/s11571-008-9047-z>
- [9] NIH. Traumatic Brain Injury: Hope Through Research. NIH Publ. No. 02-2478. Nat Inst Health (Feb. 2002).
- [10] Sokoloff L. The physiological and biochemical bases of functional brain imaging. Cogn Neurodyn 2008; 2: 1-5. <http://dx.doi.org/10.1007/s11571-007-9033-x>
- [11] Maier SE, Hardy CJ, Jolesz FA. Brain and cerebrospinal fluid motion: real-time quantification with M₀ mode MR imaging. Radiology 1994; 193(2): 477-483.
- [12] Loth F, Yardimci MA, Alperin N. Hydrodynamic modelling of cerebrospinal fluid motion within the spinal cavity. J Biomech Eng 2001; 123(1): 71-79.
- [13] Ivancevic V, Ivancevic T. Applied Differential Geometry: A Modern Introduction. World Scientific, Singapore 2007.
- [14] Ivancevic V. Symplectic Rotational Geometry in Human Biomechanics. SIAM Rev 2004; 46(3): 455-474. <http://dx.doi.org/10.1137/S003614450341313X>
- [15] Park J, Chung W-K. Geometric Integration on Euclidean Group With Application to Articulated Multibody Systems. IEEE Trans Rob 2005; 21(5): 850-863. <http://dx.doi.org/10.1109/TRO.2005.852253>
- [16] Edelen DGB. A four-dimensional formulation of defect dynamics and some of its consequences. Int J Eng Sci 1980; 18: 1095. [http://dx.doi.org/10.1016/0020-7225\(80\)90112-3](http://dx.doi.org/10.1016/0020-7225(80)90112-3)
- [17] Kadic A, Edelen DGB. A Gauge theory of Dislocations and Disclinations. Springer, New York 1983. <http://dx.doi.org/10.1007/3-540-11977-9>
- [18] McElhaney JH, Myers BS. Biomechanical Aspects of Cervical Trauma, in: Nahum AM, Melvin JW, Eds. Accidental injury: Biomechanics and Prevention, Springer, New York 1993. http://dx.doi.org/10.1007/978-1-4757-2264-2_14
- [19] Whiting WC, Zernicke RF. Biomechanics of Musculoskeletal Injury. Human Kinetics, Champaign, IL 1998.
- [20] Waddell G. The Back Pain Revolution. Churchill Livingstone, Edinburgh 1998.
- [21] Rannou F, Corvol M, Revel M, Poiraudau S. Disk degeneration and disk herniation: the contribution of mechanical stress. Joint, Bone, Spine: Revue du Rhumatisme 2001; 68(6): 543-546.
- [22] Seidel H, Griffin MJ. Modelling the response of the spinal system to whole-body vibration and repeated shock. Clin Biomech 2001; 16(1): S3-7. [http://dx.doi.org/10.1016/S0268-0033\(00\)00095-4](http://dx.doi.org/10.1016/S0268-0033(00)00095-4)
- [23] Granata KP, Marras WS. An EMG-assisted model of trunk loading during free-dynamic lifting. J Biomech 1995; 28(11): 1309-17. [http://dx.doi.org/10.1016/0021-9290\(95\)00003-Z](http://dx.doi.org/10.1016/0021-9290(95)00003-Z)
- [24] Kumar S, Narayan Y. Torque and EMG in rotation extension of the torso from pre-rotated and flexed postures. Clin Biomech 2006; 21(9): 920-931. <http://dx.doi.org/10.1016/j.clinbiomech.2006.04.017>
- [25] Reiser RF, Wickel EE, Menzer HH. Lumbar mechanics of floor to knuckle height lifting on sloped surfaces. Int J Ind Erg 2008; 38(1): 47-55. <http://dx.doi.org/10.1016/j.ergon.2007.08.002>
- [26] Ivancevic VG. Nonlinear complexity of human biodynamics engine. Nonlin Dynamics 2010; 61(1-2): 123-139. <http://dx.doi.org/10.1007/s11071-009-9636-3>
- [27] Engø K, Marthinsen A, Munthe-Kaas HZ. DiffMan- an object oriented MATLAB toolbox for solving differential equations on manifolds, Tech. Rep. 164, Dep. Informatics, Univ. Bergen, Norway 1999.
- [28] Engø K, Marthinsen A, Munthe-Kaas HZ. DiffMan User's Guide, Version 1.6, Tech. Rep. 166, Dep. Informatics, Univ. Bergen, Norway 1999.
- [29] Munthe-Kaas HZ. Lie-Butcher theory for Runge-Kutta methods. BIT 1995; 35(4): 572-587. <http://dx.doi.org/10.1007/BF01739828>
- [30] Munthe-Kaas HZ. Runge-Kutta methods on Lie groups. BIT 1998; 38(1): 92-111. <http://dx.doi.org/10.1007/BF02510919>
- [31] Munthe-Kaas HZ. High order Runge-Kutta methods on manifolds. Appl Numer Math 1999; 29: 115-127. [http://dx.doi.org/10.1016/S0168-9274\(98\)00030-0](http://dx.doi.org/10.1016/S0168-9274(98)00030-0)
- [32] Iserles A, Munthe-Kaas HZ, Nørsett SP, Zanna A. Lie-group methods. Acta Numer 2005; 9: 1-148.

Received on 09-04-2014

Accepted on 22-05-2014

Published on 20-06-2014

DOI: <http://dx.doi.org/10.12970/2308-8354.2014.02.02>

© 2014 Ivancevic and Mohamed; Licensee Synergy Publishers.

This is an open access article licensed under the terms of the Creative Commons Attribution Non-Commercial License (<http://creativecommons.org/licenses/by-nc/3.0/>) which permits unrestricted, non-commercial use, distribution and reproduction in any medium, provided the work is properly cited.